

First-principles calculations of the structural, electronic, vibrational and magnetic properties of C_{60} and $C_{48}N_{12}$: a comparative study

Rui-Hua Xie and Garnett W. Bryant

Atomic Physics Division, National Institute of Standards and Technology, Gaithersburg, MD 20899-8423

Lasse Jensen

Theoretical Chemistry, Material Science Centre, Rijksuniversiteit Groningen, Nijenborgh 4, 9747 AG Groningen, The Netherlands

Jijun Zhao

Department of Physics and Astronomy, University of North Carolina at Chapel Hill, Chapel Hill, NC 27599

Vedene H. Smith, Jr.

Department of Chemistry, Queen's University, Kingston, ON K7L 3N6, Canada

(October 22, 2018)

We perform first-principles calculations of the structural, electronic, vibrational and magnetic properties of the $C_{48}N_{12}$ azafullerene and C_{60} . Full geometrical optimization shows that $C_{48}N_{12}$ is characterized by several distinguishing features: only one nitrogen atom per pentagon, two nitrogen atoms preferentially sitting in one hexagon, S_6 symmetry, 6 unique nitrogen-carbon and 9 unique carbon-carbon bond lengths. The Mulliken charge analysis indicates that the doped nitrogen atoms in $C_{48}N_{12}$ exist as electron acceptors and three-fourths of the carbon atoms as electron donors. Electronic structure calculations of $C_{48}N_{12}$ show that the highest occupied molecular orbital (HOMO) is a doubly degenerate level of a_g symmetry and the lowest unoccupied molecular orbital (LUMO) is a nondegenerate level of a_u symmetry. The calculated binding energy per atom and HOMO-LUMO energy gap of $C_{48}N_{12}$ are about 1 eV smaller than those of C_{60} . For both $C_{48}N_{12}$ and C_{60} , the total energies calculated with STO-3G, 3-21G and 6-31G basis sets differ from the 6-31G* basis set results by about 1.5%, 0.6% and 0.05%, respectively. Because of electron correlations, the HOMO-LUMO gap decreases about 5 eV and the binding energy per atom increases about 2 eV. Our vibrational frequency analysis predicts that $C_{48}N_{12}$ has in total 116 vibrational modes: 58 modes are infrared-active (29 doubly-degenerate and 29 non-degenerate modes) and 58 modes are Raman-active (29 doubly-degenerate unpolarized and 29 non-degenerate polarized). It is found that $C_{48}N_{12}$ exhibits eight ^{13}C and two ^{15}N NMR (nuclear magnetic resonance) spectral signals. In comparison to isolated carbon or nitrogen atoms, an enhancement in the dipole polarizability is found due to the delocalized π electrons in $C_{48}N_{12}$ and C_{60} . The average second-order hyperpolarizability of $C_{48}N_{12}$ is about 55% larger than that of C_{60} . In addition, the effects of basis sets are discussed in detail, and the different methods for calculating nuclear magnetic shielding tensors are compared. Our detailed study of C_{60} reveals the importance of electron correlations and the choice of basis sets in the first-principles calculations. Our best-calculated results for C_{60} with the B3LYP hybrid density functional theory are in excellent agreement with experiment and demonstrate the desired efficiency and accuracy needed for obtaining quantitative information on the structural, electronic and vibrational properties of these molecules. Our results suggest that $C_{48}N_{12}$ has potential applications as semiconductor components, nonlinear optical materials, and possible building blocks for molecular electronics and photonic devices.

I. INTRODUCTION

Graphite is a stable and abundant solid form of pure carbon [1]. In this form, three valence electrons of each carbon atom form three strong sp^2 trigonal bonds to three nearest neighbors with an equal distance of 0.142 nm, while the fourth valence electron from different carbon atoms interacts by weak π bonds perpendicular to successive sheets with an inter-plane distance of 0.34 nm [2]. Diamond is another slightly less stable and less abundant crystallographic form of pure carbon [1], where each carbon atom is covalently bonded to four neighbors via

sp^3 hybridization at the apexes of a regular tetrahedron. In 1985, a fascinating molecule, named C_{60} (a truncated icosahedron with 20 hexagonal and 12 pentagonal faces, and 60 vertices, each of which is at the intersection of two hexagonal and one pentagonal faces) was discovered by Kroto *et al.* [3], and a new form of pure carbon, named fullerenes [4], was born.

Fullerenes can crystallize in a variety of three-dimensional structures [5,6], being made from an even number of three-coordinated sp^2 carbon atoms that arrange themselves into 12 pentagonal faces and any number (> 1) of hexagonal faces [4]. The macroscopic syn-

thesis of soot [5], which contains C_{60} and other fullerenes in large compounds, plus the straightforward purification techniques of the soot which make the pure fullerene materials available, have led to extensive studies of fullerenes [7–10,12].

Doped fullerenes have also attracted a great deal of interest due to their remarkable structural, electronic, optical and magnetic properties [7–10,12]. For example, the doped fullerenes can exhibit large third-order optical nonlinearities [9,10] and be ideal candidates as photonic devices including all-optical switching, data processing, and eye and sensor protection [9,10]. Another example is alkali-doped C_{60} crystals, which can become superconducting [13,14], for example, at a critical temperature $T_c = 30$ K [13]. In addition to the endohedral doping (inside fullerenes) and exohedral doping (outside fullerenes), there is another type of doping, named *substitutional doping*, where one or more carbon atoms of fullerene are substituted by other atoms [7–12], due to the unique structural and electronic properties of fullerenes. Because boron and nitrogen bracket carbon in the periodic table, much attention has been paid to alternate boron- and/or nitrogen-doped compounds [7–12]. Over the past 10 years, boron and nitrogen atoms have been successfully used to replace carbon atoms of C_{60} and synthesize many kinds of heterofullerenes, $C_{60-m-n}N_mB_n$ [7–10,12,15–18]. In 1995, a very efficient method of synthesizing $C_{59}N$ was reported [16]. This method has led to a number of detailed studies of the physical and chemical properties of $C_{59}N$ [8–10,12,17]. Very recently, C_{60} with more than one nitrogen atom replacing carbon atoms in the cage has been synthesized by Hultman *et al.* [18], and the existence of a novel $C_{48}N_{12}$ aza-fullerene [18–20] was reported. Hence, it would be interesting and useful to investigate and predict the structural, electronic, vibrational and magnetic properties of this aza-fullerene by performing detailed first-principles calculations. This forms main purpose of the present paper.

Fullerenes have been challenging molecules for first-principles calculations because of their size [21,22]. Recent advances in *ab initio* methods and parallel computing have brought a substantial improvement in capabilities for predicting the properties of large molecules. The coupled cluster method has been used to predict phenomena in C_{20} [24]. Other first-principles methods, which are less demanding in terms of computation cost than the coupled cluster method, have been used for much larger fullerenes and carbon nanotubes. For example, C_{60} [25–30] has been studied with self-consistent field (SCF) and Moller-Plesset second-order (MP2) theory, C_{240} [31] and carbon nanotubes [32] with density functional theory (DFT) [33,34], and C_{540} [35] with the Hartree-Fock (HF) method.

C_{60} has the highest symmetry I_h in the point group, two types of carbon-carbon (CC) bonds (one single bond C-C shared by adjacent five- and six-membered carbon rings and one double bond C=C by adjacent six-membered carbon rings), and two kinds of bond angles

(one angle between two adjacent C-C bonds, and another one between a C=C bond and a adjacent C-C bond) [7]. In section II, we perform full geometry optimizations of $C_{48}N_{12}$ as well as C_{60} with both DFT and restricted HF (RHF) methods. It is found that the $C_{48}N_{12}$ aza-fullerene has several distinguishing features: only one nitrogen atom per pentagon, two nitrogen atoms preferentially sitting in one hexagon, S_6 symmetry, six unique nitrogen-carbon (NC) and nine unique CC bonds. The Mulliken charge analysis shows that the doped nitrogen atoms in $C_{48}N_{12}$ exist as electron acceptors and three-fourths of the carbon atoms as electron donors. Our best CC bond lengths and radius of C_{60} calculated with B3LYP/6-31G* are in excellent agreement with experiment.

Total energy calculations of the optimized $C_{48}N_{12}$ and C_{60} are discussed in section III. It is found that the highest occupied molecular orbital (HOMO) is a doubly degenerate level with a_g symmetry and the lowest unoccupied molecular orbital (LUMO) is a nondegenerate level with a_u symmetry. The calculated HOMO-LUMO energy gap of $C_{48}N_{12}$ is about 1 eV smaller than that of C_{60} . For both molecules, the total energies calculated with STO-3G, 3-21G and 6-31G basis sets differ from the 6-31G* results by about 1.5%, 0.6% and 0.05%, respectively, and the HOMO-LUMO gaps decrease about 5 eV due to electron correlations. For C_{60} , our calculated results are in agreement with other groups' calculations, and our best HOMO-LUMO energy gap calculated with B3LYP/6-31G* is in agreement with experiment.

When an external electric field is applied to a molecule, its charges are redistributed and dipoles are induced or reoriented [36]. The relation between the dipole moment \mathbf{P} and the applied field \mathbf{G} can be written as [9]

$$\mathbf{P} = \mathbf{P}_0 + \alpha\mathbf{G} + \frac{\beta}{2}\mathbf{G}^2 + \frac{\gamma}{6}\mathbf{G}^3 + \dots, \quad (1)$$

where \mathbf{G} is the electric field, \mathbf{P}_0 is the permanent dipole moment, α is the dipole polarizability, β is the first-order hyperpolarizability, and γ is the second-order hyperpolarizability. The static dipole polarizability (SDP) measures the ability of the valence electrons to find a configuration which screens a static external field [9]. It has been shown that molecules with many delocalized valence electrons should display large SDPs [9,37]. The first- and second-order hyperpolarizabilities play a key role in the description of nonlinear optical phenomena since a time-varying polarization can act as the source of new components of the electromagnetic field [36]. In section IV, we calculate the SDPs and first- and second-order hyperpolarizabilities of $C_{48}N_{12}$ and C_{60} . In comparison to isolated carbon or nitrogen atoms, we find an enhancement in the SDP due to the delocalized π electrons in $C_{48}N_{12}$ and C_{60} . The calculated SDP for C_{60} is in agreement with experiment. The average second-order hyperpolarizability of $C_{48}N_{12}$ is about 55% larger than that of C_{60} .

When a material is doped, its mechanical, electronic, magnetic and optical properties change [7,9–11]. The

ability to control such induced changes is vital to progress in material science. Raman and infrared (IR) spectroscopic techniques [38,39] are useful experimental tools to investigate how doping modifies the structural and dynamical properties of the pristine material and to understand the physical origin of such induced changes. Over the past 10 years, both techniques have been used widely to study the vibrational properties of C_{60} [40–45], its derivative compounds [46–57], and (doped) carbon nanotubes [58–64]. It has been shown that C_{60} has in total 46 vibrational modes including 4 IR-active [40–43] and 10 Raman-active vibrational modes [44,45]. These studies have offered a good guide to the phonon spectrum in the solid state of these materials. In section V, we perform a vibrational analysis and calculate the infrared (IR) intensities of $C_{48}N_{12}$. Fifty eight IR-active (i.e., 29 doubly-degenerate and 29 non-degenerate modes) and 58 Raman-active (i.e., 29 doubly-degenerate unpolarized and 29 non-degenerate polarized) frequencies are determined. The best vibrational frequencies and IR results for C_{60} calculated with B3LYP are in excellent agreement with experiment and demonstrate the desirable efficiency and accuracy of this theory for obtaining quantitative information on the vibrational properties of these materials. Comparison with other groups’ calculations of C_{60} is made and discussed.

High resolution NMR [65–67] gives spectra which can be analyzed to yield parameters such as the nuclear magnetic shielding σ [68] and the nuclear spin-spin coupling J [69], which characterize molecular systems and structures. Both σ and J are determined by the electronic environments of the nuclei involved. A satisfactory theoretical description of the distribution of electrons in a molecule can lead to reliable predictions of σ and J , which have a number of applications, such as the identification of the conformation or structure of the species present in a given sample. In section VI the GIAO (gauge-including atomic orbital) [70] and the CSGT (continuous set of gauge transformations) [71] methods are utilized for calculating the nuclear magnetic shielding tensor σ in $C_{48}N_{12}$ and C_{60} at both the HF and DFT levels of theory. Eight ^{13}C and two ^{15}N NMR spectral signals are predicted for $C_{48}N_{12}$. Our best calculated NMR results for C_{60} are in excellent agreement with experiment.

Finally, we end in section VII by giving a summary and outlook on the potential applications of $C_{48}N_{12}$.

II. OPTIMIZED GEOMETRIC STRUCTURE

The geometries of both $C_{48}N_{12}$ and C_{60} were fully optimized by using the Gaussian 98 program [72,73], where we have employed both RHF and DFT methods. Also we discuss the effects of basis sets by considering STO-3G, 3-21G, 6-31G and 6-31G* [74–79]. For the DFT method, we use the B3LYP hybrid functional [80].

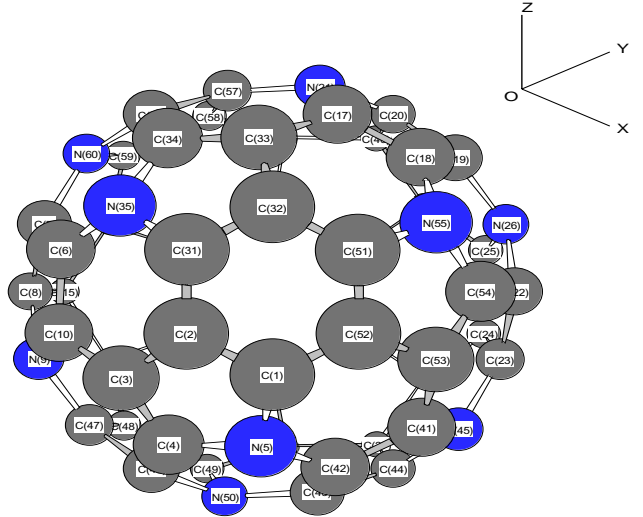


FIG.1: Geometric structure of $C_{48}N_{12}$. The site numbers $\{5, 9, 14, 21, 26, 30, 35, 39, 45, 50, 55, 60\}$ are for nitrogen atoms, while the others are for carbon atoms.

In Fig.1, we present the geometry of $C_{48}N_{12}$. The *ab initio* calculations show that $C_{48}N_{12}$ has only one nitrogen atom per pentagon and two nitrogen atoms preferentially sit in one hexagon. The symmetry of $C_{48}N_{12}$ is the S_6 point group [19,20]. The optimized distances (or radii) R_i from the i th atom to the density center of the molecule are listed in Table I. We find that there are 10 unique radii for $C_{48}N_{12}$, which suggest that $C_{48}N_{12}$ is an ellipsoidal structure and has 10 unique sites (2 for N sites and 8 for C sites), while C_{60} has an equal radius for each carbon atom. As shown in section VI, the 10 unique sites of $C_{48}N_{12}$ can be identified by NMR experiments. Comparing the B3LYP results with the RHF results shows that the radii are increased by up to 2% due to the electron correlation. Comparing the 6-31G and 6-31G*’s results shows that adding polarization functions decreases the radius of carbon sites but increases the radius of nitrogen sites. In comparison with the results of STO-3G and the split valence basis sets, we find that increasing the basis size would lead to a decreased radius. For C_{60} , the radius for each carbon site calculated by using B3LYP and the 6-31G* basis set is 3.5502 Å, which is in excellent agreement with experiment ($R = 3.55$ Å) [86], the LDA (local density approximation) calculation ($R = 3.537$ Å) with a pseudopotential approach (PPA) [87], and the LDA-based Car-Parrinello molecular dynamics (CPMD) simulation ($R = 3.55$ Å) [88]. The success of the B3LYP calculation of the C_{60} radius demonstrates the importance of electron correlation for

an accurate description of a molecular geometrical structure.

The calculated net Mulliken charges Q_i of carbon and nitrogen atoms in $C_{48}N_{12}$ are also listed in Table I. There are two unique types of nitrogen atoms in the structure. The net Mulliken charges Q_i/q ($q = 1.6 \times 10^{-19}$) on both types of N are negative, for example, -0.5953 C and -0.6002 C with B3LYP/6-31G*, -0.7803 C and -0.7829 C with RHF/6-31G*. The net Mulliken charges of the carbon atoms in $C_{48}N_{12}$ separate into two groups: 1/4 of carbon atoms with negative Q_i and the remaining 3/4 with positive Q_i . Although the Mulliken charge analysis cannot estimate the atomic charges quantitatively, their signs can be estimated [89]. From these results, we find that the doped nitrogen atoms and one-fourth of the carbon atoms exist as electron acceptors, and three-fourths of the carbon atoms as electron donors. It should be mentioned that we also performed calculations of net

Mulliken charges of carbon and boron atoms in $C_{48}B_{12}$ [90]. We found that the doped boron atoms exist as electron donors and all carbon atoms as electron acceptors [90]. Therefore, $C_{48}N_{12}$ and $C_{48}B_{12}$ have opposite electronic polarizations, while C_{60} is isotropic. In the case of doping into silicon, the V family in the periodic table (for example, phosphorous) exists as a donor, while the III family (for example, boron) exists as an electron acceptor. Thus, the B- or N-substituted doping in C_{60} differs greatly from that for silicon. This is due to the unique structural and electronic properties of C_{60} [7]. With respect to the electron correlation and the choice of basis sets, we find that the absolute value of the net Mulliken charge Q_i for each atom in $C_{48}N_{12}$ increases with an increase of the basis size, but decreases due to the electron correlation or by adding polarization functions to a given basis set.

Table I: Net Mulliken charge Q_i ($q = 1.6 \times 10^{-19}$) and radius R_i ($1 \text{ \AA} = 0.1 \text{ nm}$) at the site number n_i in $C_{48}N_{12}$ and C_{60} calculated by RHF and B3LYP methods with a variety of Pople-style basis sets.

Method	Fullerene	Site Number $\{n_i\}$	Atom	STO-3G		3-21G		6-31G		6-31G*			
				R_i [\AA]	Q_i/q [C]	R_i [\AA]	Q_i/q [C]	R_i [\AA]	Q_i/q [C]	R_i [\AA]	Q_i/q [C]		
RHF	$C_{48}N_{12}$	{ 1, 13, 16, 31, 38, 51 }	C	3.5452	0.1073	3.5059	0.3856	3.5082	0.3546	3.4988	0.2926		
		{ 2, 12, 29, 32, 37, 52 }	C	3.5591	-0.0238	3.5299	-0.0897	3.5271	-0.0515	3.5162	-0.0621		
		{ 3, 11, 28, 33, 36, 53 }	C	3.5602	-0.0192	3.5353	-0.0609	3.5275	-0.0344	3.5389	-0.0480		
		{ 4, 15, 27, 34, 40, 54 }	C	3.5331	0.0942	3.4954	0.3905	3.4999	0.3701	3.4716	0.3167		
		{ 5, 14, 30, 35, 39, 55 }	N	3.6974	-0.2406	3.5691	-0.9541	3.5685	-0.9552	3.6151	-0.7803		
		{ 6, 18, 24, 42, 48, 58 }	C	3.4292	0.0601	3.4229	0.2907	3.4299	0.2758	3.3880	0.2209		
		{ 7, 19, 23, 43, 47, 57 }	C	3.4023	0.0893	3.3874	0.3363	3.3983	0.3058	3.3409	0.2962		
		{ 8, 20, 22, 44, 46, 56 }	C	3.4723	0.0718	3.4599	0.3191	3.4577	0.3522	3.4416	0.2433		
		{ 9, 21, 26, 45, 50, 60 }	N	3.5870	-0.2344	3.4985	-0.9878	3.4951	-0.9913	3.5082	-0.7829		
		{ 10, 17, 25, 41, 49, 59 }	C	3.4851	0.0952	3.4586	0.3703	3.4631	0.3737	3.4222	0.3036		
		C_{60}	{ 1, 2, 3, 4, 5, 6, ..., 60 }	C	3.5473	0	3.5238	0	3.5300	0	3.5226	0	
		B3LYP	$C_{48}N_{12}$	{ 1, 13, 16, 31, 38, 51 }	C	3.5871	0.0827	3.5302	0.2770	3.5365	0.2147	3.5171	0.1961
				{ 2, 12, 29, 32, 37, 52 }	C	3.5923	-0.0188	3.5469	-0.0422	3.5458	-0.0175	3.5275	-0.0125
{ 3, 11, 28, 33, 36, 53 }	C			3.6019	-0.0193	3.5533	-0.0358	3.5492	-0.0173	3.5395	-0.0298		
{ 4, 15, 27, 34, 40, 54 }	C			3.5951	0.0682	3.5381	0.2861	3.5408	0.2486	3.5190	0.2266		
{ 5, 14, 30, 35, 39, 55 }	N			3.7175	-0.1883	3.5918	-0.7543	3.5945	-0.6690	3.6187	-0.5953		
{ 6, 18, 24, 42, 48, 58 }	C			3.5092	0.0550	3.4592	0.2522	3.4706	0.1985	3.4348	0.1919		
{ 7, 19, 23, 43, 47, 57 }	C			3.4882	0.0679	3.4328	0.2635	3.4465	0.2103	3.4049	0.2124		
{ 8, 20, 22, 44, 46, 56 }	C			3.5431	0.0618	3.4917	0.2637	3.4946	0.2623	3.4720	0.1998		
{ 9, 21, 26, 45, 50, 60 }	N			3.6302	-0.1814	3.5336	-0.7787	3.5304	-0.7047	3.5335	-0.6002		
{ 10, 17, 25, 41, 49, 59 }	C			3.5554	0.0723	3.5056	0.2686	3.5087	0.2548	3.4807	0.2110		
C_{60}	{ 1, 2, 3, 4, 5, 6, ..., 60 }			C	3.6034	0	3.5555	0	3.5615	0	3.5502	0	

Table II: Bond lengths (L, 1 Å = 0.1 nm) in C₄₈N₁₂ and C₆₀ calculated by using B3LYP methods with a variety of Pople-style basis sets, where (n_i, n_j) denotes the site number pair that forms a bond.

Fullerene	Bond	(n _i , n _j)	STO-3G		3-21G		6-31G		6-31G*	
			L _{df_t} [Å]	L _{r_hf} [Å]	L _{df_t} [Å]	L _{r_hf} [Å]	L _{df_t} [Å]	L _{r_hf} [Å]	L _{df_t} [Å]	L _{r_hf} [Å]
C ₄₈ N ₁₂	CC	(1, 2) (12, 13) (16, 29) (31, 32) (37, 38) (51, 52)	1.4275	1.3914	1.4103	1.3855	1.4125	1.3880	1.4061	1.3836
	CC	(1, 52) (2, 31) (12, 38) (13, 29) (16, 37) (32, 51)	1.4371	1.4151	1.4171	1.4083	1.4216	1.4134	1.4155	1.4024
	NC	(1, 5) (13, 14) (16, 30) (31, 35) (38, 39) (51, 55)	1.4742	1.4601	1.432	1.4206	1.4315	1.4164	1.4300	1.4272
	CC	(2, 3) (11, 12) (28, 29) (32, 33) (36, 37) (52, 53)	1.4701	1.4662	1.4517	1.4524	1.4488	1.4478	1.4455	1.4521
	CC	(3, 4) (11, 15) (27, 28) (33, 34) (36, 40) (53, 54)	1.4092	1.3590	1.3947	1.3620	1.3971	1.3652	1.3901	1.3588
	CC	(3, 10) (11, 59) (17, 33) (25, 36) (28, 49) (41, 53)	1.4559	1.4566	1.4320	1.4350	1.4346	1.4367	1.4314	1.4368
	NC	(4, 5) (14, 15) (27, 30) (39, 40) (34, 35) (54, 55)	1.4707	1.4553	1.4307	1.4128	1.4286	1.4108	1.4224	1.4047
	CC	(4, 46) (8, 15) (20, 40) (22, 54) (27, 44) (34, 56)	1.4567	1.4589	1.4326	1.4367	1.4354	1.4388	1.4313	1.4372
	NC	(5, 42) (6, 35) (14, 48) (18, 55) (24, 30) (39, 58)	1.4749	1.4637	1.4299	1.4294	1.4317	1.4278	1.4287	1.4310
	CC	(6, 7) (18, 19) (23, 24) (42, 43) (47, 48) (57, 58)	1.4399	1.4352	1.4211	1.4182	1.4217	1.4185	1.4136	1.4143
	CC	(6, 10) (17, 18) (24, 25) (58, 59) (41, 42) (48, 49)	1.4119	1.3641	1.3963	1.3664	1.4004	1.3712	1.3941	1.3634
	CC	(7, 8) (19, 20) (22, 23) (43, 44) (46, 47) (56, 57)	1.4195	1.3705	1.4021	1.3718	1.4068	1.3761	1.4021	1.3703
	NC	(7, 60) (9, 47) (19, 26) (21, 57) (23, 45) (43, 50)	1.4586	1.4419	1.4159	1.4047	1.4189	1.4071	1.4099	1.3958
	NC	(8, 9) (20, 21) (22, 26) (44, 45) (46, 50) (56, 60)	1.4510	1.4313	1.4182	1.4083	1.4149	1.4012	1.4084	1.4056
	NC	(9, 10) (17, 21) (25, 26) (41, 45) (49, 50) (59, 60)	1.4612	1.4360	1.4271	1.4043	1.4226	1.3997	1.4134	1.3919
	C ₆₀	C=C	(1, 52) (2, 31) (3, 10) ...	1.4130	1.3759	1.3899	1.3671	1.3981	1.3750	1.3949
C-C		(1, 2) (1, 5) (2, 3) ...	1.4773	1.4628	1.4601	1.4529	1.4592	1.4524	1.4539	1.4487

The optimized CC and NC bond lengths in C₄₈N₁₂ are listed in Table II. We find that there are 6 unique NC and 9 unique CC bonds. In comparison with the calculated CC bond lengths for C₆₀ shown in Table II, the CC bond length in C₄₈N₁₂, in general, is less than the single C-C bond length of C₆₀ due to the redistribution of the electron density. It is also found that the bond length increases due to the electron correlation, but decreases as we increase the basis size or include the polarization function.

In comparison with experimental data available for C₆₀ listed in Table III, we find that the two kinds of bond lengths of C₆₀ calculated by using the B3LYP with a large basis set 6-31G* are in good agreement with the results measured by X-ray powder diffraction (XRPD) [91], NMR [92,93], gas-phase electron diffraction (GPED) [94] or X-ray crystallography technique (XRCT) [86].

For comparison, Table III also lists the calculated CC bond lengths for C₆₀ with a selection of previous theoretical calculations. Given the low computational cost of Hückel theory, the bond lengths [95] predicted by this theory are remarkably satisfactory. The semi-empirical QCFF/PI (quantum-chemical-force-fields for π electrons) [96] does not predict as good bond lengths as the Hückel theory since it has been parameterized mainly with respect to frequencies of conjugated hydrocarbons. The CC bond lengths calculated by using the semi-empirical MNDO (modified neglect of differential overlap) [97] and the extended Hubbard model (EHM) [98] are a little improved. These theoretical approaches empirically include the effect of electron correlation found in conjugated π -systems. The HF [25–27,30] and SCFMO (self-consistent field with MO) [29] calculations are in agreement with our RHF results. As listed in Table III,

the calculated MP2 bond distances [28] usually decrease by about 0.01 Å when more d functions are added to the basis set, demonstrating the necessity of including polarization functions in calculations with correlation. Based on the differences between the HF and MP2 data, it is evident that electron correlation effects should be considered in an accurate description of the equilibrium structure of a molecule. The CC bond lengths calculated with the LDA [99–101], LDA-PPA [87], and LDA-based CPMD simulation [88,102] are in agreement with our B3LYP’s results and demonstrate the importance of electron correlation effects in giving accurately the equilibrium structure of a molecule.

Table III: Equilibrium CC bond lengths (1 Å = 0.1 nm) of C_{60} from previous theoretical predictions and experimental findings. STO-DZP and DNP denote double-zeta STO’s and double numerical basis with polarization functions, respectively.

Method	C-C [Å]	C=C [Å]	Reference
Hückel	1.436	1.418	[95]
QCFF/PI	1.471	1.411	[96]
MNDO	1.465	1.376	[97]
EHM	1.446	1.402	[98]
SCFMO	1.49	1.43	[29]
HF/STO-3G	1.463	1.376	[25]
HF/3-21G	1.453	1.367	[30]
HF/DZ	1.451	1.368	[26]
HF/STO-3G	1.463	1.376	[27]
HF/DZ	1.451	1.368	[27]
HF/DZP	1.450	1.375	[27]
HF/TZP	1.448	1.370	[27]
MP2/DZ	1.470	1.407	[28]
MP2/DZP	1.451	1.412	[28]
MP2/TZP	1.446	1.406	[28]
LDA/STO-DZP	1.436	1.384	[101]
LDA/DZP	1.445	1.395	[100]
LDA/DNP	1.444	1.391	[99]
LDA-PPA	1.449	1.390	[87]
LDA-CPMD	1.45	1.40	[88]
LDA-CPMD	1.45	1.39	[102]
Exp./XRCT	1.4459	1.3997	[86]
Exp./XRPD	1.455	1.391	[91]
Exp./NMR	1.45	1.40	[92]
Exp./NMR	1.46	1.40	[93]
Exp./GPED	1.458	1.401	[94]

As mentioned before, C_{60} has only two kinds of bond angles [7], 108° (the angle between two adjacent single C-C bonds) and 120° (the angle between a double C=C bond and an adjacent single C-C bond). Fig.2(a-d)

show the distribution of (C-C-C, C-N-C, C-C-N) bond angles in $C_{48}N_{12}$ calculated by using both RHF and B3LYP methods with several different basis sets. One-third and two-thirds of the bond angles in $C_{48}N_{12}$ fluctuate around 108° and 120° , respectively. Comparing Fig.2(a) and 2(b) shows that increasing the basis size leads to smaller fluctuations in the bond angle distribution (BAD) around either 108° or 120° . In comparison with Fig.2(b), Fig.2(c) exhibits enhanced fluctuations in the BAD as polarization functions are added to the 6-31G basis set. Comparing Fig.2(c) with Fig.2(d), we find that the BAD in $C_{48}N_{12}$ are decreased due the effect of electron correlation.

III. TOTAL ELECTRONIC ENERGY

We performed total energy calculations of $C_{48}N_{12}$ and C_{60} by using both RHF and B3LYP with STO-3G, 3-21G, 6-31G and 6-31G* basis sets. The results are summarized in Table IV. The orbital energies are shown in Fig.3, where the orbital symmetries are also labeled.

Table IV demonstrates the convergence of the total energy calculations of both RHF and B3LYP methods with respect to the basis sets. For both $C_{48}N_{12}$ and C_{60} , the total energies calculated with STO-3G, 3-21G and 6-31G basis sets differ from the 6-31G* basis set results by about 1.5%, 0.6% and 0.05%, respectively. For both molecules, comparing the B3LYP and RHF results shows that the HOMO-LUMO energy gap Δ decreases about 5 eV and the binding energy E_b per atom increases about 2 eV because of the electron correlations. The calculated binding energy E_b per atom and HOMO-LUMO energy gap Δ of $C_{48}N_{12}$ are about 1 eV smaller than those of C_{60} .

Because of the valency of the doped nitrogen atoms, the electronic properties of $C_{48}N_{12}$ and C_{60} are significantly different. As shown in Fig.3(a) and Fig.3(b), the HOMO for C_{60} is fivefold-degenerate with h_u symmetry, the LUMO is threefold-degenerate with t_{1u} symmetry, and the others are threefold-degenerate with t_{1g} or t_{2u} symmetry, fourfold-degenerate with g_g or g_u symmetry, and fivefold-degenerate with h_g symmetry. We notice from Fig.3 that each energy level in $C_{48}N_{12}$ splits since the icosahedral symmetry of C_{60} is lost by the substitutional doping. For $C_{48}N_{12}$, the HOMO is a doubly degenerate level of a_g symmetry, the LUMO is a non-degenerate level with a_u symmetry, and the others are specified in Fig.3. Considering that $C_{48}N_{12}$ is isoelectronic with C_{60}^{-12} , we find that the filling of the energy levels in $C_{48}N_{12}$ corresponds to a complete filling of the t_{1u} and t_{1g} levels of C_{60} .

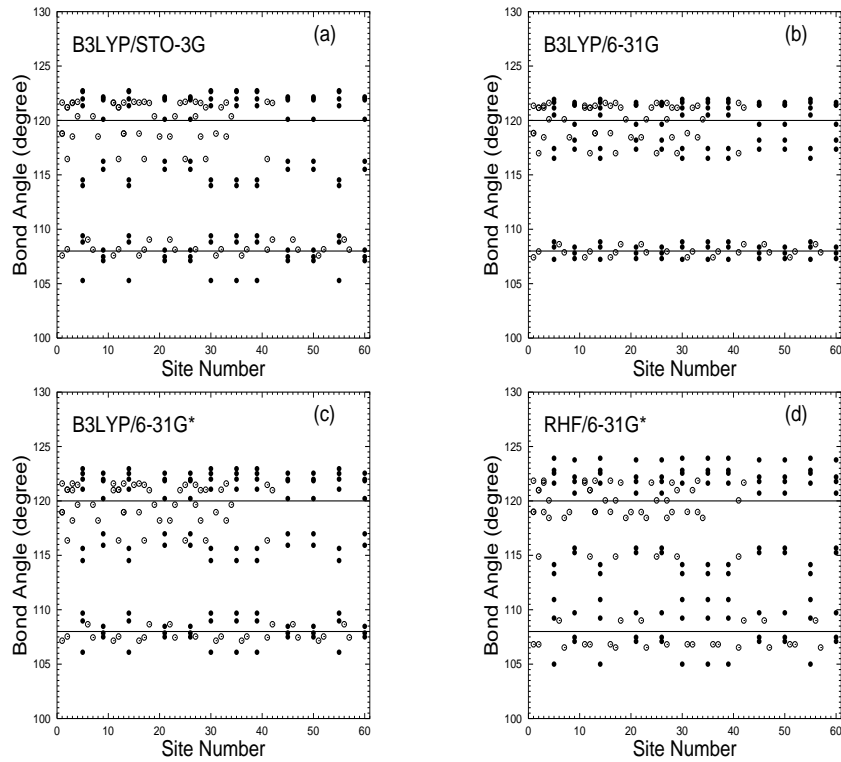


FIG.2: *Ab initio* calculations of C-C-C (open circles) and C-N-C (or C-C-N) (filled circles) bond angles in $C_{48}N_{12}$: (a) B3LYP/STO-3G; (b) B3LYP/6-31G; (c) B3LYP/6-31G*; (d) RHF/6-31G*. The site numbers are labeled as in Fig.1. The solid lines are the C-C-C bond angles (108° and 120°) of C_{60} .

Table IV: Total electronic energy (E_t , in eV), LUMO energy (E_{lumo} , in eV), HOMO energy (E_{homo} , in eV), HOMO-LUMO energy gap (Δ , in eV), binding energy per atom (E_b , in eV), ionization potential (E_{IP} , in eV) and electron affinity (E_{EA} , in eV) of $C_{48}N_{12}$ and C_{60} calculated by using RHF and B3LYP methods with a variety of Pople-style basis sets.

Method	Energy	C_{60}				$C_{48}N_{12}$			
		STO-3G	3-21G	6-31G	6-31G*	STO-3G	3-21G	6-31G	6-31G*
RHF	E_t	-61067.132	-61471.413	-61795.062	-61817.394	-66397.387	-66846.232	-67193.956	-67223.547
	E_{lumo}	2.688	-0.632	-0.709	-0.117	3.797	0.499	0.214	0.643
	E_{homo}	-5.456	-8.323	-7.919	-7.644	-3.287	-6.506	-6.203	-6.189
	Δ	8.144	7.691	7.210	7.527	7.084	7.005	6.417	6.832
	E_b	5.581	4.627	4.666	4.956	4.510	3.734	3.724	4.149
	E_{IP}	4.892	8.230	5.685	5.659	2.45	6.144	5.314	5.530
	E_{EA}	2.280	0.881	1.187	1.125	1.947	0.146	0.209	0.267
B3LYP	E_t	-61446.662	-61864.864	-62194.006	-62209.002	-66795.835	-67263.771	-67617.031	-67637.724
	E_{lumo}	-1.127	-3.563	-3.390	-3.219	-0.188	-2.783	-2.706	-2.614
	E_{homo}	-4.356	-6.509	-6.221	-5.987	-2.365	-4.743	-4.633	-4.383
	Δ	3.229	2.946	2.831	2.768	2.177	1.96	1.927	1.774
	E_b	7.715	6.786	6.843	6.982	6.888	6.140	6.088	6.365
	E_{IP}	3.868	7.814	8.576	7.317	2.488	6.040	5.600	5.663
	E_{EA}	1.487	2.295	1.073	2.398	0.804	1.514	0.223	1.493

In Table IV, we list the calculated ionization potential (IP) E_{IP} and electron affinity (EA) E_{EA} for both C_{60} and $C_{48}N_{12}$. It shows that $C_{48}N_{12}$ is a good electron donor, while C_{60} is a good electron acceptor. The calculated IP for C_{60} is in good agreement with the experiments: (7.54 ± 0.01) eV [103], (7.57 ± 0.01) eV [104], $(7.58^{+0.04}_{-0.02})$ eV [105], and (7.59 ± 0.02) eV [106]. The calculated EA for C_{60} agrees well with the experiments: (2.666 ± 0.001) eV [107], (2.689 ± 0.008) eV [108].

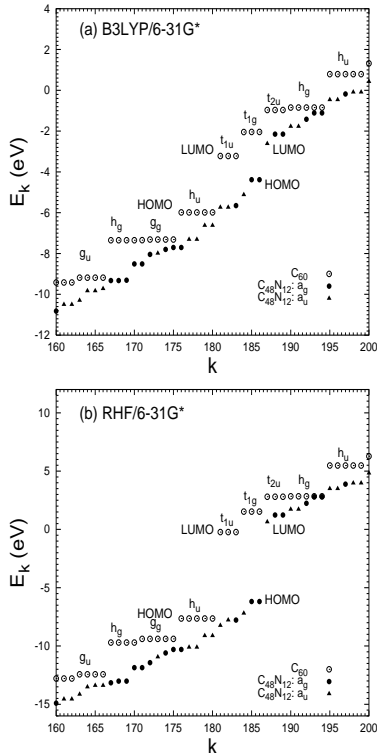


Fig.3: Orbital energies E_k of the k th eigenstate of C_{60} and $C_{48}N_{12}$ calculated with (a) B3LYP/6-31G* and (b) RHF/6-31G*. Open circles are for C_{60} . Filled circles and triangles are for $C_{48}N_{12}$, respectively. The orbital symmetries of energy levels are shown.

For comparison, here we list the total energies of C_{60} for a selection of previous theoretical calculations. Using the HF methods, Scuseria [27] found that the total energies of C_{60} calculated with DZ, DZP and TZP basis sets [25–27,30] are -61745.723 eV, -61826.192 eV and -61832.443 eV, respectively. These results are in agreement with our RHF calculations. Moreover, using the MP2 method, Scuseria and colleagues [28] have shown that the total energies of C_{60} with DZ, DZP and TZP basis sets are -61893.398 eV, -61826.192 eV and -61832.443 eV, respectively. The total energies calculated by using the MP2 method do improve the approximation made in HF method. This result demonstrates that electron correlation effects cannot be neglected for an accurate prediction of the total energy of a molecule.

In crystals, the on-site Coulomb interaction between two electrons on the same molecule is given by [109]

$$U = U_{free} - 2E_p, \quad (2)$$

$$U_{free} = E_{IP} - E_{EA} - \Delta, \quad (3)$$

where $E_p = z\alpha e^2/(2L^4)$ (z : the number of nearest neighbors, L : the distance between molecules, α : the dipole polarizability) is the polarization energy and U_{free} is the on-site Coulomb interaction between two electrons on the free molecule [7]. Our plane-wave pseudopotential calculations performed by using the CASTEP program [73,110] show that the optimized lattice constants for C_{60} and $C_{48}N_{12}$ -based fcc solids (note: $z = 12$ for both cases) are all around 1.45 nm, while the experimental lattice constant = 1.4161 nm for C_{60} [111]. Based on our first principles results for E_{IP} , E_{EA} and Δ for C_{60} and $C_{48}N_{12}$ molecules, we arrive at the value of the on-site Coulomb interaction, $U = 1.84, 2.05$ eV for C_{60} and $C_{48}N_{12}$ solids, respectively. The experimental values for C_{60} are $U = 1.6 \pm 0.2$ eV [109] and 1.54 eV [112]. Moreover, our DFT/GGA calculations show that the band gap E_{gap} for the $C_{48}N_{12}$ solid is about 0.85 eV smaller than that of C_{60} . This is consistent with the Δ - U - W relation [7]

$$E_{gap} = \Delta + U - W, \quad (4)$$

where W is the bandwidth for the HOMO- or LUMO-derived energy bands. Assuming the same W for both $C_{48}N_{12}$ and C_{60} solids, we arrive at

$$E_{gap}^{C_{48}N_{12}} \approx E_{gap}^{C_{60}} - 0.79 \text{ eV}. \quad (5)$$

The DFT is known to underestimate the band gap of solids. From experiment, $E_{gap} = 2.3 \pm 0.1$ eV [109] and 2.86 eV [112] for the C_{60} solid. Hence, using the approximate relation given by Eq.(5), we obtain an estimated band gap for the $C_{48}N_{12}$ fcc solid of $E_{gap}^{C_{48}N_{12}} = 1.7 \pm 0.3$ eV. Thus, the $C_{48}N_{12}$ solid, like C_{60} , is a semiconducting material.

Similarly, we find that the $C_{48}B_{12}$ -based fcc solid (lattice constant ≈ 1.45 nm) is also a semiconducting material [90], having $U = 1.9$ eV, $E_{gap}^{C_{48}B_{12}} - E_{gap}^{C_{60}} = -1.34$ eV, and $E_{gap}^{C_{48}B_{12}} = 1.2 \pm 0.3$ eV.

IV. STATIC (HYPER)POLARIZABILITY

The static polarizabilities for $C_{48}N_{12}$ and C_{60} are presented in Table V. The B3LYP and RHF results are obtained by using the Gaussian 98 program package [72,73] and the LDA results by using the ADF (Amsterdam Density Functional) program [73,113,114]. The ADF program uses basis sets of Slater functions, where a triple zeta valence basis plus polarization is augmented with the field-induced polarization (FIP) functions of Zeiss et al. [115]. Here this basis set is denoted as TZP++ ([6s4p2d1f] for C and N atoms, and [4s2p1d] for H atom)

and has recently been used for calculating the second-order hyperpolarizabilities, γ , for C_{60} , $C_{58}N_2$, $C_{58}B_2$ and $C_{58}BN$ [116].

From the results listed in Table V, we see that the basis set dependence is identical for both B3LYP and RHF cases. As expected, improving the basis set increases the polarizability. Our RHF results for C_{60} are in good agreement with a previous study [117] which used a similar method and basis sets. The B3LYP values are about 10% larger than the corresponding RHF values. The LDA results are much larger than both the B3LYP and RHF results. This is expected since the basis set is larger and expected to predict a more accurate polarizability

[116]. Also LDA, in general, predicts a larger polarizability than does with B3LYP [118]. The LDA results for C_{60} are in good agreement with previous LDA studies [119–121]. We find that the polarizability of $C_{48}N_{12}$ is slightly smaller than the polarizability of C_{60} . For $C_{48}N_{12}$ we also find that the zz component is slightly larger than the xx component except when using RHF and a small basis set. In comparison with the SDP of a single carbon or nitrogen atom, we find an enhanced linear polarizability for both C_{60} and $C_{48}N_{12}$. This is expected since both molecules have many conjugate π electrons delocalized over the entire system.

Table V: Static polarizabilities (α , in $\text{\AA}^3 = 10^{-30} \text{ m}^3$) for $C_{48}N_{12}$ and C_{60} with RHF and DFT methods and a variety of basis sets. Symmetry relations give for C_{60} , $\alpha_{xx} = \alpha_{yy} = \alpha_{zz}$, and for $C_{48}N_{12}$, $\alpha_{xx} = \alpha_{yy}$.

	STO-3G		3-21G		6-31G		6-31G*		TZP++
	B3LYP	RHF	B3LYP	RHF	B3LYP	RHF	B3LYP	RHF	LDA
C_{60}									
α_{xx}	52.5	45.2	64.9	59.5	68.3	63.2	69.5	64.7	84.7
$C_{48}N_{12}$									
α_{xx}	51.5	43.5	62.0	55.6	65.6	59.4	66.6	60.0	79.3
α_{zz}	51.6	41.6	62.6	54.9	66.1	58.5	67.5	60.4	81.5

Table VI: Static 2nd-order hyperpolarizabilities (γ , in au. $1 \text{ au} = 6.235378 \times 10^{-65} \text{ C}^4\text{m}^4\text{J}^{-3}$) for $C_{48}N_{12}$ and C_{60} calculated using LDA and TZP++. The average 2nd-order hyperpolarizability is given by $\bar{\gamma} = \frac{1}{15} \sum_{i,j} (\gamma_{iijj} + \gamma_{ijij} + \gamma_{ijji})$. Symmetry relations give $\gamma_{xxxx} = \gamma_{yyyy}$, $\gamma_{xxzz} = \gamma_{yyzz}$ and $\gamma_{zzxx} = \gamma_{zzyy}$.

	γ_{xxxx}	γ_{xyxy}	γ_{zzzz}	γ_{xxzz}	γ_{zzxx}	$\bar{\gamma}$
C_{60}	137950	45983	137950	45983	45983	137950
$C_{48}N_{12}$	188780	62880	232970	85120	84790	215222

Because C_{60} is well separated in a crystal [7], one can model the fullerene crystal in an electric field as a collection of isolated dipoles. For such systems, the Clausius-Mossotti relation [122] is expected to yield a reasonably accurate relationship between the linear polarizability of an isolated molecule and the dielectric constant of a fullerene crystal, i.e.,

$$|\alpha| = \frac{3(\epsilon - 1)}{4\pi\rho_f(\epsilon + 2)}, \quad (6)$$

where ρ_f is the density of fullerene molecules in a fcc crystal and ϵ is the dielectric constant of the fullerene crystal. For the purposes of comparison, we note that Hebard *et al.* [123] and Ecklund [124] measured the dielectric constants of C_{60} films in the range between 3.9 and 4.0. Based on these measured dielectric constants, one can derive an experimental polarizability of about $84.9 \times 10^{-30} \text{ m}^3$ for C_{60} (the density $\rho_f = 10^{30}/712 \text{ m}^{-3}$ is given by Quong and Pederson [125]). Very recently, using the molecular beam deflection technique, Antoine *et*

al. [126] have measured the electric polarizability of isolated C_{60} molecules and obtained a value of $(76.5 \pm 8.0) \times 10^{-30} \text{ m}^3$. Using a new optical technique that uses light forces and a time-of-flight spectrometer, Ballard *et al.* [127] have made absolute measurements of cluster polarizabilities and determined the optical polarizability of C_{60} at the fundamental wavelength of a Nd:YAG laser ($\lambda = 1064 \text{ nm}$) to be $(79 \pm 4) \times 10^{-30} \text{ m}^3$. The experimental results are in good agreement with our LDA results, especially considering that LDA is expected to overestimate the polarizability.

The static first-order hyperpolarizability β [36] of the $C_{48}N_{12}$ molecule is also calculated and found to be zero, the same as that for C_{60} molecule. This is expected since both $C_{48}N_{12}$ and C_{60} molecule display inversion symmetries. Consequently, this aza-fullerene cannot produce second-order nonlinear optical interactions.

The static 2nd-order hyperpolarizabilities for $C_{48}N_{12}$ and C_{60} molecules are presented in Table VI. For the calculations of the 2nd-order hyperpolarizability,

γ , we use time-dependent (TD) DFT as described in Ref. [116,120,128,129]. First, the 1st-order hyperpolarizability, β , is calculated analytically in the presence of a small electric field. Then, the 2nd-order hyperpolarizability can be obtained by a finite-field differentiation of the analytically calculated 1st-order hyperpolarizability. For all the TD-DFT calculations we used the RESPONSE code [73,128,130] implemented in the ADF program [73,113,114]. The small difference between γ_{xxxx} and γ_{zzxx} for $C_{48}N_{12}$ is due to the numerical method adopted for calculating γ .

For the γ value of C_{60} , we find good agreement with previous first-principles results [120,121,131]. A comparison with experiments will not be made for the 2nd-order hyperpolarizability due to large differences in the experimental results [9,10,120,131]. We find that all components of the 2nd-order hyperpolarizability for $C_{48}N_{12}$ are larger than for C_{60} . This gives an average 2nd-order hyperpolarizability of $C_{48}N_{12}$ which is about 55 % larger than the average 2nd-order hyperpolarizability of C_{60} . The $zzzz$ components of the 2nd-order hyperpolarizability of $C_{48}N_{12}$ is also larger than that found in the donor/acceptor substituted $C_{58}BN$ molecule [116].

V. VIBRATIONAL FREQUENCY ANALYSIS

A. Theory

To lowest order, IR intensities are proportional to the derivatives of the dipole moment with respect to the vibrational normal modes of the material, evaluated at the equilibrium geometry. In detail, the IR intensity of the q th vibrational mode is given by [132]

$$I_{IR}^{(q)} = \frac{\rho_p \pi}{3c} \left| \frac{d\mathbf{P}}{d\Xi_q} \right|^2, \quad (7)$$

where ρ_p is the particle density, Ξ_q is the normal coordinate corresponding to the q th mode and c is the velocity of light. Since $|d\mathbf{P}/d\Xi_q|$ is the only molecular property entering the formula, it is often referred to as absolute IR intensity.

To obtain the IR data, one must compute the derivatives of the dipole moment with respect to the normal mode coordinates. These can be viewed as directional derivatives in the space of $3N$ nuclear coordinates and expressed in terms of derivatives with respect to atomic coordinates, R_k . For the i th component of the dipole moment \mathbf{P} ($i=x,y,z$), we have

$$\frac{d\mathbf{P}_i}{d\Xi_q} = \sum_{k=1}^{3N} \frac{\partial \mathbf{P}_i}{\partial R_k} \xi_{kq}, \quad (8)$$

where $\xi_{kq} = \partial R_k / \partial \Xi_q$ is the k th atomic displacement of the q th normal mode. Then, the necessary derivatives can be expressed in terms of the atomic forces as follows [132,133]

$$\frac{\partial \mathbf{P}_i}{\partial R_k} = - \frac{\partial^2 E}{\partial G_i \partial R_k} = \frac{\partial F_k}{\partial G_i}, \quad (9)$$

where E is the total energy, G_i is the i th component of an assumed external electric field \mathbf{G} , and F_k is the calculated force on the k th atomic coordinate.

B. Normal Vibrations in C_{60} and $C_{48}N_{12}$

Using the Gaussian 98 program [72,73], we calculated the harmonic vibrational frequencies of both C_{60} and $C_{48}N_{12}$ and considered the effects of the basis sets. It should be mentioned that our frequencies have not been scaled.

Table VII and VIII summarize the vibrational frequencies for C_{60} calculated by using RHF and B3LYP methods, respectively. As shown by Dresselhaus *et al.* [134], there are 46 vibrational modes for C_{60} . These modes are classified in even and odd parities and in ten irreducible representatives of the I_h point group: the $\{a_g, a_u\}$, $\{t_{1g}, t_{1u}, t_{2g}, t_{2u}\}$, $\{g_g, g_u\}$ and $\{h_g, h_u\}$ modes are non-, threefold-, fourfold- and fivefold-degenerate, respectively. Tables VII and VIII demonstrate that increasing the basis size improves the accuracy of the predicted vibrational frequencies, but adding polarization functions to the 6-31G basis set only improves slightly the accuracy of the vibrational frequencies. In choosing a basis set for the first-principles calculation, one must make a compromise between accuracy and CPU time. Our results shows that the minimum calculation can be done in about 4 hours of CPU, while the most expensive calculation requires 12 days of CPU. Without significant computational cost, one can do B3LYP/STO-3G calculation and still obtain results more accurate than any RHF calculations. Going beyond STO-3G for B3LYP calculations requires a drastic increase in CPU time. Surprisingly, going just to 3-21G provides the most accurate results, while for the bigger basis set 6-31G, the results are worse and adding a polarized function to 6-31G only slightly improves the results. The 3-21G basis set gives systematically lower frequencies than the 6-31G basis set, while the frequencies obtained from the 6-31G* basis set typically lie between the results of the other two basis sets. In contrast, as discussed in section II, 6-31G* does provide the most accurate bond lengths. This suggests that the better accuracy of 3-21G is fortuitous. Increasing the basis set to 6-31G stiffens the bonds, while adding the polarization function compensates by softening the bonds. In comparison with the B3LYP results, RHF calculated frequencies are too high due to an incorrect description of bond dissociation, while B3LYP with large basis sets (even the minimum basis set STO-3G) generally gives results in good agreement with the experiments of Wang *et al.* [42] and Dong *et al.* [47]. This demonstrates the importance of electron correlation in an accurate description of the vibrational frequencies.

For comparison, Table VII lists the vibrational frequencies of C_{60} calculated by using various theories, for example, the semi-empirical MNDO [97] and QCFF/PI [96] methods. Of these, the QCFF/PI method, which has been parameterized mainly with respect to vibrational frequencies of conjugated and aromatic hydrocarbons [135], results in the best results although it gives less satisfactory geometry. Such accurate prediction implies that the electronic structures of C_{60} is not much different from other aromatic hydrocarbons [96]. Häser *et al.* [28] showed that the approximate harmonic frequencies for the two a_g vibrational modes of C_{60} are 1615 cm^{-1} and 487 cm^{-1} for HF/DZP, 1614 cm^{-1} and 483 cm^{-1} for HF/TZP, 1614 cm^{-1} and 437 cm^{-1} for MP2/DZP, and 1586 cm^{-1} and 437 cm^{-1} for MP2/TZP. Their HF calculations are in agreement with our RHF/3-21G results. Their MP2 results are more accurate when obtained with large basis sets, which also demonstrates the importance of electron correlation in predicting the vibrational frequencies.

In addition, there have been a number of 2nd nearest-neighbor force-constant models (FCMs) [136–138] which have been used to calculate the phonon frequencies of C_{60} . None of them yield good agreement with the experimental data. For example, an empirical force field, which has been parameterized with respect to polycyclic aromatic hydrocarbons, is used with Hückel theory and predicts vibrational frequencies of the two a_g modes of 1409 cm^{-1} and 388 cm^{-1} [137] that are too low. However, the modified FCM (MFCM) by Jishi *et al.* [139] considered interactions up to the third-nearest neighbors, and the calculated results, as shown in Table VII, are in excellent agreement with the experiments of Wang *et al.* [42] and Dong *et al.* [47].

Table VIII also lists the vibrational frequencies of C_{60} calculated by other DFT methods, for example, LDA-PPA [87], LDA [100,101] and DFT-LDA-based CPMD simulations [102]. In general, those calculated results are in good agreement with experiment. Very recently, Choi *et al.* [141] have performed B3LYP vibrational calculations of C_{60} with a 3-21G basis set but involving scaling of the internal force constants (SIFC) \tilde{K}_{ij}^{int} by using Pulay’s method [142], i.e.,

$$\tilde{K}_{ij}^{scaled} = (s_i s_j)^{1/2} \tilde{K}_{ij}^{int}, \quad (10)$$

where \tilde{K}_{ij}^{int} is the force constant in internal coordinates (the Gaussian 98 program [72] uses this form), and s_i and s_j are scaling factors for the i th and j th redundant internal coordinates, respectively. They optimized the scaling factors by minimizing the root-mean-square deviations between the experimental and calculated scaled frequencies. Their results are listed in Table IX. Overall, their scaling procedure improves the accuracy for the 46 vibrational frequencies of C_{60} , especially, for the a_g , h_g and t_{1u} vibrational modes.

In Table X and XI, we list the vibrational frequencies for $C_{48}N_{12}$ calculated with RHF and B3LYP methods

and a variety of Pople-style basis sets. In contrast with C_{60} , it is found that there are in total 116 vibrational modes for $C_{48}N_{12}$ because of its lowered symmetry, S_6 . These vibrational modes are classified into 58 doubly-degenerate and 58 nondegenerate modes. Among those vibrational modes, there are 58 IR-active (listed in Table X) and 58 Raman-active modes (listed in Table XI). Table X and XI show that the electron correlation or increasing the basis size results in a redshift of the vibrational frequencies. This is similar to that of C_{60} .

C. IR Intensities in $C_{48}N_{12}$ and C_{60}

We perform calculations of IR intensities I_{IR} for both $C_{48}N_{12}$ and C_{60} by using the Gaussian 98 program [72,73] with RHF and B3LYP methods. The calculated IR intensities for C_{60} at the corresponding frequencies are listed in Table XII, and those for $C_{48}N_{12}$ are shown in Fig.4.

For C_{60} , we note that its IR spectrum is very simple. Namely, it is composed of 4 IR-active vibrational modes with t_{1u} symmetry. This is a consequence of the symmetry of the icosahedral group [134]. Carbon clusters of comparable size, but lower symmetry, have many more IR-active frequencies. For example, the graphite isomer of C_{60} has D_{6h} symmetry and 20 IR-active frequencies [97]. Other examples [97] included C_{54} , a planar graphite fragment with D_{6h} symmetry and 22 IR-active frequencies, and C_{50} , a spheroidal cluster with D_{5h} symmetry and 22 IR-active frequencies. From Table XII, we see that the IR intensity of a given mode decreases due to the electron correlation and converges with increasing basis size. We find that our intensities calculated with B3LYP agree reasonably with experimental spectrum [140] obtained by *in situ* high-resolution FTIR measurement of a C_{60} film.

The IR intensities I_{IR} at the corresponding vibrational frequencies for $C_{48}N_{12}$ are presented in Fig.4(a)(b)(c) for calculations with B3LYP/STO-3G, B3LYP/3-21G and RHF/3-21G, respectively. As discussed above, $C_{48}N_{12}$ has 29 nondegenerate and 29 doubly-degenerate IR-active vibrational modes. Similar to the case of C_{60} , the IR signals separate into two regions, i.e., a high-frequency ($> 1000\text{ cm}^{-1}$) and a low-frequency ($\leq 1000\text{ cm}^{-1}$) region. The IR-active frequencies are redshifted by including the electron correlation or increasing the basis size. The IR intensities decrease after including electron correlations and converge with increasing basis size. The strongest IR spectral lines in both low- and high-frequency regions are the doubly-degenerate modes located, for example, at 440 cm^{-1} and 1310 cm^{-1} , respectively, for the B3LYP/3-21G case. Since experimental IR spectroscopic data do not directly indicate the specific type of nuclear motion producing each IR peak, we do not give here the normal mode information for each vibrational frequency and the displacements of each nuclei corresponding to each normal mode. In Fig.5, taking

B3LYP/3-21G calculations as an example, we only show the vibrational displacements of sites 1 to 5 (4 C sites and 1 N site) for the strongest IR spectral signals in the low-

and high-frequency regions. It is seen that the pentagon structure for the low-frequency case expands slightly and

Table VII: Vibrational frequencies (ν , in cm^{-1}) of C_{60} calculated with RHF and a variety of Pople-style basis sets. Numbers in the parenthesis are the relative errors to the experimental frequencies, ν^{exp} , from Wang *et al.* [42] and Dong *et al.* [47]. The approximated CPU times for STO-3G, 3-21G, 6-31G and 6-31G* basis sets are 5 hours, 12 hours, 18 hours and 39 hours, respectively. Results of other theoretical calculations, for example, QCFF/PI [96], MNDO [97] and MFCM [139], are also listed.

Mode	STO-3G	3-21G	6-31G	6-31G*	QCFF/PI	MFCM	MNDO	Exp.
Even Parity								
a_g	1684 (14.5%)	1604 (9.1%)	1637 (11.3%)	1600 (8.9%)	1442 (1.9%)	1468 (0.1%)	1667 (13.4%)	1470
	553 (11.0%)	518 (4.0%)	526 (5.7%)	527 (5.7%)	513 (3.0%)	492 (1.2%)	610 (22.5%)	498
g_g	1802 (18.2%)	1667 (9.3%)	1697 (11.3%)	1687 (10.6%)	1585 (3.9%)	1521 (0.3%)	1650 (8.2%)	1525
	1531 (12.9%)	1426 (5.1%)	1450 (6.9%)	1441 (6.3%)	1450 (6.9%)	1375 (1.4%)	1404 (3.5%)	1356
	1203 (11.8%)	1095 (1.8%)	1142 (6.2%)	1132 (5.2%)	1158 (7.6%)	1056 (1.9%)	1235 (14.8%)	1076
	908 (12.6%)	787 (2.3%)	878 (9.0%)	836 (3.8%)	770 (4.5%)	805 (0.1%)	856 (6.2%)	806
	653 (5.2%)	646 (4.1%)	643 (3.5%)	619 (0.3%)	614 (1.1%)	626 (0.8%)	579 (6.9%)	621
h_g	574 (18.0%)	529 (9.0%)	549 (12.9%)	537 (10.5%)	476 (2.1%)	498 (2.5%)	491 (1.0%)	486
	1912 (21.2%)	1772 (12.3%)	1799 (14.0%)	1791 (13.5%)	1644 (4.2%)	1575 (0.2%)	1722 (9.1%)	1578
	1658 (16.2%)	1546 (8.4%)	1585 (11.1%)	1562 (9.4%)	1465 (2.7%)	1401 (1.8%)	1596 (11.8%)	1427
	1482 (18.4%)	1326 (6.0%)	1377 (10.1%)	1380 (10.3%)	1265 (1.1%)	1217 (2.7%)	1407 (12.5%)	1251
	1290 (17.2%)	1184 (7.5%)	1208 (9.8%)	1208 (9.7%)	1154 (4.8%)	1102 (0.1%)	1261 (14.5%)	1101
	886 (14.3%)	828 (6.9%)	843 (8.6%)	840 (8.4%)	801 (3.4%)	788 (1.7%)	924 (19.2%)	775
	836 (17.6%)	761 (7.1%)	821 (15.4%)	794 (11.7%)	691 (2.8%)	708 (0.4%)	771 (8.4%)	711
	509 (17.5%)	475 (9.7%)	496 (14.5%)	482 (11.4%)	440 (1.6%)	439 (1.4%)	447 (3.2%)	433
t_{1g}	302 (10.7%)	295 (8.0%)	296 (8.3%)	289 (5.9%)	258 (5.5%)	269 (1.5%)	263 (3.7%)	273
	1505 (10.9%)	1371 (0.9%)	1403 (3.3%)	1404 (3.4%)	1398 (2.9%)	1346 (0.9%)	1410 (3.8%)	1358
	966 (1.0%)	940 (3.7%)	939 (3.8%)	916 (6.1%)	975 (0.1%)	981 (0.5%)	865 (11.4%)	976
t_{2g}	687 (36.9%)	618 (23.1%)	670 (33.4%)	640 (27.5%)	597 (18.9%)	501 (0.2%)	627 (24.9%)	502
	1619 (19.1%)	1453 (6.9%)	1504 (10.6%)	1511 (11.1%)	1470 (8.1%)	1351 (0.7%)	1483 (9.0%)	1360
	912 (0.2%)	907 (0.8%)	898 (1.8%)	868 (5.0%)	890 (2.6%)	931 (1.8%)	919 (0.5%)	914
	903 (4.3%)	701 (19.0%)	828 (4.3%)	734 (15.1%)	834 (3.6%)	847 (2.1%)	784 (9.4%)	865
	647 (14.1%)	637 (12.3%)	634 (11.7%)	613 (8.1%)	637 (12.3%)	541 (4.6%)	591 (4.2%)	567
Odd Parity								
a_u	1111 (2.8%)	1112 (2.5%)	1097 (4.1%)	1061 (7.2%)	1206 (5.5%)	1142 (0.1%)	972 (15.0%)	1143
g_u	1701 (17.7%)	1562 (8.0%)	1607 (11.1%)	1597 (10.4%)	1546 (6.9%)	1413 (2.3%)	1587 (9.8%)	1446
	1527 (16.6%)	1406 (7.3%)	1447 (10.5%)	1437 (9.7%)	1401 (6.9%)	1327 (1.3%)	1436 (9.6%)	1310
	1113 (14.7%)	1031 (6.3%)	1052 (8.4%)	1050 (8.3%)	1007 (3.8%)	961 (0.9%)	1110 (4.1%)	970
	922 (0.2%)	859 (7.0%)	864 (6.5%)	826 (10.6%)	832 (10.0%)	929 (0.5%)	914 (1.1%)	924
	863 (13.5%)	738 (2.9%)	846 (11.4%)	786 (3.4%)	816 (7.4%)	789 (3.8%)	750 (1.3%)	760
h_u	414 (3.5%)	390 (2.4%)	400 (0.1%)	390 (2.4%)	358 (10.5%)	385 (3.8%)	362 (9.5%)	400
	1905 (22.2%)	1762 (13.0%)	1791 (14.9%)	1784 (14.5%)	1646 (5.6%)	1552 (0.4%)	1709 (9.6%)	1559
	1597 (15.3%)	1447 (4.5%)	1487 (7.4%)	1491 (7.7%)	1469 (6.1%)	1385 (0.0%)	1467 (5.9%)	1385
	1453 (30.0%)	1320 (18.2%)	1353 (21.2%)	1354 (21.2%)	1269 (13.6%)	1129 (1.1%)	1344 (20.3%)	1117
	886 (10.5%)	793 (1.0%)	858 (7.1%)	824 (2.8%)	812 (1.4%)	801 (0.0%)	822 (2.6%)	801
	777 (11.7%)	753 (8.2%)	761 (9.3%)	738 (6.0%)	724 (4.0%)	700 (0.6%)	706 (1.4%)	696
	640 (13.6%)	587 (4.2%)	613 (8.9%)	592 (5.2%)	531 (5.7%)	543 (3.6%)	546 (3.0%)	563
	463 (35.0%)	455 (32.7%)	454 (32.4%)	442 (28.7%)	403 (17.5%)	361 (5.0%)	403 (17.5%)	343
t_{1u}	1637 (14.5%)	1553 (8.6%)	1587 (11.0%)	1549 (8.4%)	1437 (0.6%)	1450 (1.5%)	1628 (13.9%)	1429
	1396 (18.0%)	1245 (5.2%)	1287 (8.8%)	1297 (9.6%)	1212 (2.5%)	1208 (2.1%)	1353 (14.4%)	1183
	656 (13.9%)	614 (6.5%)	623 (8.1%)	625 (8.5%)	637 (10.6%)	589 (2.3%)	719 (24.8%)	576
t_{2u}	627 (18.9%)	575 (9.1%)	621 (17.8%)	599 (13.6%)	544 (3.2%)	505 (4.2%)	577 (9.5%)	527
	1828 (15.9%)	1709 (8.4%)	1728 (9.5%)	1713 (8.6%)	1558 (1.2%)	1575 (0.1%)	1687 (7.0%)	1577
	1327 (29.3%)	1214 (1.1%)	1259 (4.5%)	1257 (4.7%)	1241 (3.3%)	1212 (0.9%)	1314 (9.4%)	1201
	1074 (4.7%)	995 (3.1%)	1025 (0.1%)	1014 (1.2%)	999 (2.6%)	1025 (0.1%)	1134 (10.5%)	1026
	835 (22.8%)	765 (12.6%)	830 (22.1%)	799 (17.5%)	690 (1.5%)	677 (0.4%)	776 (14.1%)	680
	393 (10.5%)	377 (5.9%)	385 (8.0%)	372 (4.5%)	350 (1.7%)	367 (3.1%)	348 (2.2%)	356

Table VIII: Vibrational frequencies ν (cm^{-1}) of C_{60} calculated by using the B3LYP method with a variety of Pople-style basis sets. Numbers in the parenthesis are the relative errors of the calculated frequencies to the experimental frequencies listed in Table VII. The approximated CPU times for STO-3G, 3-21G, 6-31G and 6-31G* basis sets are 4 hours, 5 days, 8 days and 12 days, respectively. The other theoretical results are from Bohnen *et al.* [87], Dixon *et al.* [100], Hara *et al.* [101], and Onida *et al.* [102].

Mode	STO-3G	3-21G	6-31G	6-31G*	Hara	Dixon	Onida	Bohnen
Even Parity								
a_g	1549 (5.4%)	1501 (2.1%)	1524 (3.7%)	1504 (2.3%)	1531 (4.1%)	1525 (3.7%)	1447 (1.6%)	1475 (0.3%)
	502 (0.9%)	491 (1.4%)	496 (0.4%)	489 (1.8%)	502 (0.8%)	499 (0.2%)	482 (3.2%)	481 (3.4%)
g_g	1594 (4.5%)	1524 (0.1%)	1546 (1.4%)	1538 (0.9%)	1538 (0.9%)	1548 (1.5%)	1479 (3.0%)	1501 (1.6%)
	1380 (1.8%)	1323 (2.4%)	1342 (1.0%)	1334 (1.6%)	1337 (1.4%)	1347 (0.7%)	1314 (3.1%)	1287 (5.1%)
	1127 (4.7%)	1062 (1.3%)	1099 (2.1%)	1093 (1.6%)	1123 4.4(%)	1122 (4.3%)	1047 (2.7%)	1037 (3.6%)
	788 (2.2%)	690 (14.4%)	777 (3.7%)	754 (6.5%)	759 (5.8%)	788 (2.2%)	781 (3.1%)	772 (4.2%)
	592 (4.6%)	598 (3.7%)	594 (4.3%)	577 (7.1%)	579 (6.8%)	573 (7.7%)	594 (4.3%)	570 (8.2%)
	508 (4.6%)	484 (0.4%)	500 (2.9%)	489 (0.7%)	486 (0.0%)	484 (0.4%)	482 (0.8%)	480 (1.2%)
h_g	1677 (6.3%)	1609 (2.0%)	1627 (3.1%)	1618 (2.5%)	1609 (2.0%)	1618 (2.5%)	1573 (0.3%)	1580 (0.1%)
	1500 (5.1%)	1436 (0.6%)	1466 (2.8%)	1455 (1.9%)	1475 (3.4%)	1475 (3.4%)	1394 (2.3%)	1422 (0.4%)
	1332 (6.5%)	1231 (1.6%)	1274 (1.8%)	1275 (1.9%)	1288 (3.0%)	1297 (3.7%)	1208 (3.4%)	1198 (4.2%)
	1166 (5.9%)	1112 (1.0%)	1129 (2.6%)	1125 (2.2%)	1129 (2.5%)	1128 (2.5%)	1098 (0.3%)	1079 (2.0%)
	802 (3.5%)	781 (0.8%)	788 (1.7%)	766 (1.2%)	794 (2.5%)	788 (1.7%)	775 (0.0%)	763 (1.5%)
	734 (3.3%)	678 (4.7%)	738 (3.8%)	718 (0.9%)	711 (0.0%)	727 (2.3%)	730 (2.7%)	716 (0.7%)
	449 (3.7%)	429 (1.0%)	448 (3.5%)	436 (0.8%)	430 (0.7%)	431 (0.5%)	435 (0.5%)	422 (2.5%)
	271 (0.6%)	271 (0.8%)	272 (0.5%)	266 (2.7%)	269 (1.5%)	261 (4.4%)	261 (4.4%)	263 (3.7%)
t_{1g}	1357 (0.1%)	1278 (5.9%)	1303 (4.0%)	1301 (4.2%)	1305 (3.9%)	1318 (2.9%)	1284 (5.4%)	1241 (8.6%)
	865 (11.3%)	865 (11.4%)	858 (12.1%)	840 (13.9%)	842 (13.7%)	830 (15.0%)	847 (13.2%)	826 (15.4%)
t_{2g}	594 (18.3%)	544 (8.3%)	593 (18.1%)	576 (14.8%)	565 (12.5%)	579 (15.3%)	580 (15.5%)	563 (10.8%)
	1431 (5.2%)	1330 (2.2%)	1372 (0.8%)	1370 (0.7%)	1370 (0.7%)	1393 (2.4%)	1257 (7.6%)	1277 (6.1%)
	827 (9.5%)	839 (8.2%)	829 (9.3%)	804 (12.0%)	809 (11.5%)	839 (8.2%)	816 (10.7%)	800 (12.5%)
	809 (6.4%)	650 (24.9%)	766 (11.4%)	743 (14.1%)	765 (11.6%)	804 (7.1%)	789 (8.8%)	788 (8.9%)
	581 (2.5%)	586 (3.3%)	582 (2.6%)	566 (0.1%)	566 (0.2%)	551 (2.8%)	559 (1.4%)	543 (4.4%)
Odd Parity								
a_u	994 (13.0%)	1013 (11.4%)	991 (13.3%)	982 (14.1%)	968 (15.3%)	972 (15.0%)	934 (18.3%)	973 (14.9%)
g_u	1513 (4.7%)	1435 (0.8%)	1470 (1.7%)	1461 (1.0%)	1474 (1.9%)	1480 (2.4%)	1395 (3.5%)	1420 (1.8%)
	1381 (5.4%)	1303 (0.5%)	1338 (2.1%)	1333 (1.7%)	1345 (2.7%)	1359 (3.7%)	1289 (1.6%)	1259 (3.9%)
	1009 (4.1%)	972 (0.2%)	985 (1.5%)	977 (0.7%)	989 (2.0%)	984 (1.4%)	939 (3.2%)	937 (3.4%)
	815 (11.8%)	795 (14.0%)	788 (14.7%)	787 (14.8%)	780 (15.6%)	830 (10.2%)	796 (13.9%)	790 (14.5%)
	784 (3.1%)	666 (12.4%)	775 (2.0%)	751 (1.2%)	762 (0.3%)	762 (0.3%)	763 (0.4%)	756 (0.5%)
	368 (8.1%)	359 (10.3%)	366 (8.4%)	357 (10.7%)	355 (11.3%)	350 (12.5%)	352 (12.0%)	348 (13.0%)
h_u	1668 (7.0%)	1596 (2.4%)	1617 (3.7%)	1608 (3.2%)	1598 (2.5%)	1611 (3.3%)	1545 (0.9%)	1566 (0.4%)
	1427 (3.0%)	1340 (3.2%)	1371 (1.0%)	1369 (11.8%)	1371 (1.0%)	1389 (0.3%)	1314 (5.1%)	1291 (6.8%)
	1295 (16.0%)	1219 (9.1%)	1246 (11.6%)	1243 (11.3%)	1243 (11.3%)	1248 (11.7%)	1198 (7.3%)	1175 (5.2%)
	771 (3.7%)	719 (10.3%)	763 (4.7%)	736 (8.1%)	742 (7.4%)	762 (4.9%)	769 (4.0%)	750 (6.4%)
	696 (0.1%)	674 (3.2%)	697 (0.1%)	679 (2.5%)	677 (2.7%)	671 (3.6%)	672 (3.4%)	661 (5.0%)
	564 (0.1%)	532 (5.5%)	555 (1.4%)	540 (4.1%)	537 (4.6%)	541 (3.9%)	540 (4.1%)	527 (6.4%)
	417 (21.5%)	419 (22.1%)	418 (21.8%)	408 (19.0%)	411 (19.8%)	401 (16.9%)	404 (17.8%)	388 (13.1%)
	1505 (5.3%)	1454 (1.7%)	1479 (3.5%)	1464 (2.4%)	1489 (4.2%)	1486 (4.0%)	1399 (2.1%)	1457 (2.0%)
t_{1u}	1266 (7.0%)	1175 (0.6%)	1209 (2.2%)	1212 (2.5%)	1222 (3.3%)	1224 (3.5%)	1158 (2.1%)	1143 (3.4%)
	596 (3.4%)	582 (0.9%)	587 (1.8%)	570 (1.0%)	595 (3.3%)	591 (2.6%)	566 (1.7%)	569 (1.2%)
	546 (3.6%)	508 (3.6%)	553 (4.9%)	537 (1.8%)	528 (0.2%)	535 (1.5%)	541 (2.7%)	514 (2.5%)
	t_{2u}	1622 (2.8%)	1568 (0.6%)	1579 (0.2%)	1568 (0.6%)	1568 (0.6%)	1571 (0.4%)	1537 (2.5%)
1235 (2.8%)		1163 (3.2%)	1201 (0.0%)	1199 (0.2%)	1231 (2.5%)	1234 (2.7%)	1108 (7.7%)	1131 (5.8%)
1002 (2.4%)		964 (6.0%)	984 (4.1%)	966 (5.9%)	997 (2.8%)	996 (2.9%)	936 (8.8%)	945 (7.9%)
734 (7.9%)		678 (0.3%)	742 (9.2%)	722 (6.1%)	715 (5.1%)	726 (6.8%)	774 (13.8%)	725 (6.6%)
354 (0.5%)		345 (3.1%)	352 (4.3%)	342 (4.0%)	343 (3.7%)	342 (3.9%)	340 (4.5%)	343 (3.8%)

Table IX: Vibrational frequencies ν (cm^{-1}) of C_{60} obtained by Choi *et al.* [141] using B3LYP/3-21G but involving scaling of the internal force constant by using Pulay’s method. Numbers in the parenthesis are the relative errors of the calculated frequencies to the experimental frequencies listed in Table VII.

Even Parity						Odd Parity					
Mode	ν	Mode	ν	Mode	ν	Mode	ν	Mode	ν	Mode	ν
a_g	1470 (0.0%)			t_{1g}	1290 (5.0%)	a_u	1078 (5.7%)			t_{1u}	1433 (0.3%)
	495 (0.6%)	h_g	1576 (0.1%)		904 (7.4%)						1180 (0.3%)
			1427 (0.0%)		565 (12.5%)			h_u	1567 (0.5%)		577 (0.2%)
g_g	1497 (1.8%)		1251 (0.0%)			g_u	1429 (1.2%)		1343 (3.0%)		526 (0.2%)
	1348 (0.6%)		1101 (0.0%)				1315 (0.4%)		1214 (8.7%)	t_{2u}	1524 (3.4%)
	1040 (3.3%)		775 (0.0%)	t_{2g}	1340 (1.5%)		970 (0.0%)		737 (8.0%)		1142 (5.0%)
	758 (6.0%)		711 (0.0%)		831 (9.1%)		797 (13.7%)		694 (0.3%)		955 (6.9%)
	592 (4.7%)		431 (0.5%)		668 (22.8%)		707 (7.0%)		535 (5.0%)		716 (5.3%)
	485 (0.2%)		267 (2.2%)		614 (8.3%)		354 (11.5%)		403 (17.5%)		340 (4.5%)

Table X: Fifty eight IR-active frequencies (ν , in cm^{-1}) of $\text{C}_{48}\text{N}_{12}$ calculated by using RHF and B3LYP methods with a variety of Pople-style basis sets.

Doubly-degenerate Modes								Non-degenerate Modes							
B3LYP				RHF				B3LYP				RHF			
STO-3G	3-21G	6-31G	6-31G*	STO-3G	3-21G	6-31G	6-31G*	STO-3G	3-21G	6-31G	6-31G*	STO-3G	3-21G	6-31G	6-31G*
314	308	318	309	358	338	350	344	286	287	297	287	305	303	317	305
363	359	369	357	400	386	398	381	328	318	329	325	370	350	362	361
394	404	406	395	430	431	436	419	362	359	371	360	404	394	406	392
406	412	418	406	452	452	454	443	391	402	406	395	428	434	437	423
437	422	441	425	513	472	495	479	450	413	447	431	527	466	498	482
465	440	464	446	551	497	523	506	470	454	467	460	556	505	524	522
496	469	491	481	578	532	554	549	581	567	580	579	641	603	617	614
566	558	569	570	619	591	606	604	592	600	639	611	695	662	720	662
623	585	633	606	723	662	707	671	645	609	653	622	735	709	739	705
632	635	662	639	738	730	741	719	656	654	674	645	767	734	747	722
656	665	679	658	763	747	755	735	692	698	707	686	802	762	779	755
675	686	697	675	771	767	786	757	735	709	722	700	839	800	819	770
695	701	709	695	801	783	801	779	784	798	798	778	871	859	867	836
722	721	729	712	843	810	829	807	798	809	803	786	899	878	879	853
788	804	800	782	879	871	874	847	958	963	968	961	1058	1035	1044	1030
973	958	965	954	1072	1028	1040	1020	972	977	982	967	1076	1055	1062	1045
1055	1041	1050	1040	1162	1118	1135	1116	990	1010	993	976	1095	1102	1092	1060
1203	1136	1163	1159	1336	1217	1259	1244	1057	1042	1056	1047	1165	1125	1145	1124
1231	1172	1199	1197	1372	1265	1301	1292	1220	1142	1171	1177	1351	1232	1272	1272
1275	1210	1237	1237	1415	1304	1341	1334	1276	1215	1238	1229	1393	1311	1345	1330
1348	1280	1306	1302	1501	1369	1409	1397	1331	1252	1277	1270	1446	1326	1365	1351
1391	1311	1339	1340	1552	1413	1454	1450	1362	1293	1318	1317	1464	1381	1421	1377
1440	1354	1387	1389	1618	1467	1512	1511	1421	1345	1380	1384	1521	1405	1463	1412
1478	1410	1448	1437	1647	1511	1562	1540	1437	1374	1413	1394	1609	1451	1502	1494
1525	1443	1476	1473	1731	1566	1613	1605	1466	1381	1422	1418	1621	1490	1532	1533
1555	1475	1502	1499	1769	1612	1652	1642	1506	1418	1458	1461	1700	1523	1583	1574
1602	1521	1553	1553	1839	1673	1713	1713	1560	1497	1529	1518	1773	1633	1674	1662
1628	1544	1578	1576	1855	1693	1735	1748	1617	1516	1549	1555	1872	1692	1731	1748
1680	1592	1625	1624	1941	1760	1801	1808	1627	1542	1574	1575	1894	1701	1742	1751

Table XI: Fifty eight Raman-active frequencies (ν , in cm^{-1}) for $\text{C}_{48}\text{N}_{12}$ calculated by using RHF and B3LYP methods with a variety of Pople-style basis sets.

Doubly-degenerate Modes								Non-degenerate Modes							
B3LYP				RHF				B3LYP				RHF			
STO-3G	3-21G	6-31G	6-31G*	STO-3G	3-21G	6-31G	6-31G*	STO-3G	3-21G	6-31G	6-31G*	STO-3G	3-21G	6-31G	6-31G*
245	248	252	245	263	262	268	261	264	264	268	264	294	288	291	288
259	261	265	260	286	281	286	281	382	368	389	376	445	406	429	388
376	368	387	371	429	409	428	413	406	398	415	398	463	415	448	425
410	388	409	396	470	433	455	440	444	415	442	424	510	455	483	454
447	429	446	437	514	479	497	488	471	458	477	467	523	491	511	489
493	450	482	472	583	517	549	540	498	491	500	495	576	521	543	524
549	568	566	551	604	610	611	592	544	505	544	510	608	566	587	575
580	596	597	581	652	647	650	629	578	588	592	576	646	637	640	615
617	613	652	627	725	699	736	706	585	598	602	588	650	651	652	637
649	629	662	641	773	726	759	741	621	603	616	597	723	655	670	652
665	671	698	671	780	762	785	757	625	614	652	627	744	705	749	716
716	695	714	699	831	776	807	788	658	657	684	656	777	760	784	738
767	760	768	766	848	820	833	821	730	690	709	689	832	779	802	773
782	776	782	780	871	844	853	840	768	765	773	766	867	825	836	819
841	865	860	843	935	943	944	918	836	851	844	830	924	918	919	897
858	887	877	854	961	974	966	933	856	881	869	844	953	965	956	916
1124	1084	1105	1093	1238	1160	1192	1164	1115	1080	1100	1092	1216	1165	1192	1175
1162	1123	1141	1138	1281	1197	1225	1215	1194	1160	1173	1162	1328	1244	1264	1251
1182	1147	1163	1156	1313	1238	1262	1250	1221	1181	1196	1189	1344	1260	1281	1273
1274	1186	1220	1223	1423	1276	1325	1318	1316	1241	1267	1265	1400	1335	1374	1348
1318	1243	1274	1272	1476	1341	1383	1377	1337	1253	1280	1279	1469	1347	1389	1377
1386	1311	1337	1336	1546	1421	1457	1449	1367	1293	1322	1320	1498	1375	1424	1380
1452	1369	1407	1404	1608	1468	1517	1503	1416	1347	1383	1379	1534	1415	1468	1429
1466	1388	1420	1420	1647	1490	1537	1540	1439	1373	1415	1397	1583	1437	1485	1476
1504	1415	1452	1451	1717	1541	1591	1587	1481	1419	1453	1441	1655	1528	1578	1552
1571	1489	1517	1515	1781	1631	1671	1664	1531	1440	1477	1477	1721	1560	1612	1602
1595	1516	1551	1551	1831	1670	1710	1720	1558	1487	1511	1505	1766	1612	1649	1626
1633	1544	1578	1578	1883	1708	1749	1759	1581	1509	1545	1530	1817	1644	1687	1680
1662	1578	1610	1610	1916	1735	1778	1788	1683	1592	1624	1623	1946	1767	1804	1809

Table XII: RHF and B3LYP calculations of IR intensities (I_{IR} , in 10^3m/mole) of C_{60} with the corresponding vibrational modes and frequencies (ν , in cm^{-1}).

Method	Mode	STO-3G		3-21G		6-31G		6-31G*	
		I_{IR}	ν	I_{IR}	ν	I_{IR}	ν	I_{IR}	ν
B3LYP	t_{1u}	10.6	1505	14.0	1454	17.2	1479	15.6	1464
		21.0	1266	9.2	1175	10.1	1209	8.9	1212
		0.5	596	5.9	582	8.2	587	10.7	570
		22.0	546	28.8	508	27.7	553	27.1	537
RHF	t_{1u}	11.5	1637	16.5	1553	24.5	1587	17.1	1549
		25.1	1396	11.4	1245	11.8	1287	10.6	1297
		0.6	656	6.0	614	14.7	623	10.4	625
		35.9	627	42.1	575	34.3	621	48.0	599

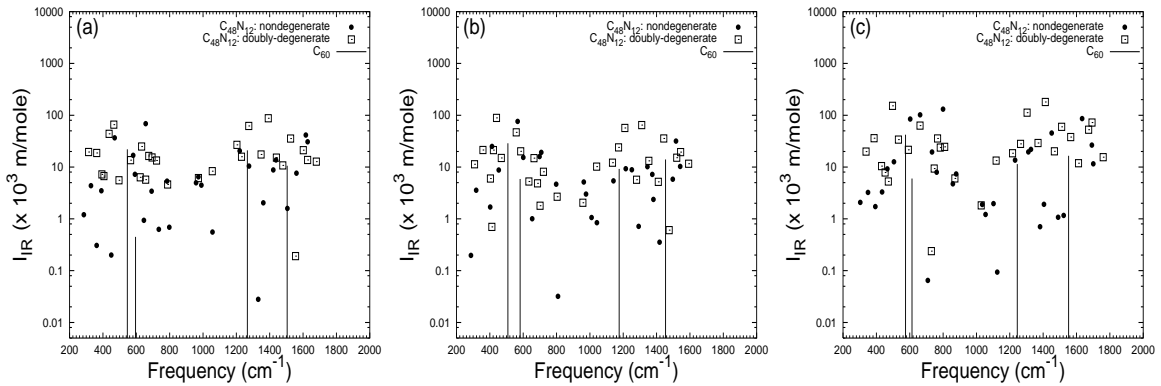


FIG.4: *Ab initio* calculation of IR intensity (I_{IR} , in 10^3 m/mole) at its corresponding frequency in $C_{48}N_{12}$: (a) B3LYP/STO-3G; (b) B3LYP/3-21G; (c) RHF/3-21G. The solid lines are the calculated results for C_{60} .

shows collective vibration along the z-x direction, while the pentagon structure for the high-frequency case contracts, accompanying a large stretching of site 3 along the z direction.

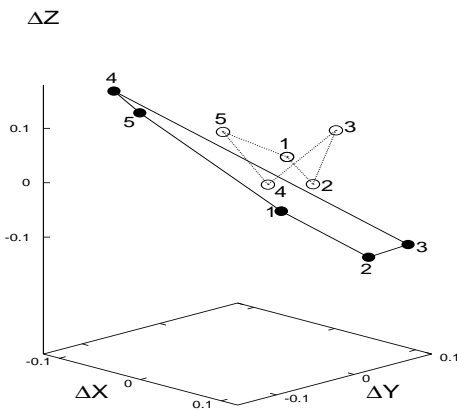


FIG.5: The vibrational displacements of sites 1 to 5 for the strongest IR spectral signals of $C_{48}N_{12}$ in the low-frequency (filled circles) and high-frequency (open circles) regions for the B3LYP/3-21G case.

VI. NUCLEAR MAGNETIC SHIELDING TENSORS

A. Theoretical Methods

There are a number of theoretical methods for calculating the second-order magnetic response properties of molecules. It has been shown that gauge-invariant procedures (GIPs) [71,143] are required to predict accurately these properties within a finite basis approximation. In

this paper, we focus on using two GIPs, i.e., the gauge-including atomic orbital (GIAO) procedure and the continuous set of gauge transformations (CSGT) procedure, to predict NMR shielding tensors at the Hartree-Fock and DFT levels of theory. GIAO and CSGT achieve gauge-invariance in different ways. The GIAO method uses basis functions having explicit field dependence [70], whereas the CSGT method achieves the gauge-invariance by performing a continuous set of gauge transformations. Ditchfield [144] first adopted the GIAO method to perform quantum chemical NMR shift calculations and the CSGT method was developed by Keith and Bader [71]. In the following, we briefly introduce the two methods. More details can be found, for example, in the works of Cheeseman *et al.* [145] and Wolinski *et al.* [146].

It is known that the nuclear magnetic shielding tensor can be written as the mixed second derivative of the energy E with respect to the external magnetic field \mathbf{B} and the magnetic moment \mathbf{I} of nucleus X :

$$\sigma_{ik} = \frac{\partial^2 E}{\partial I_i \partial B_k}, \quad (11)$$

where B_k and I_i are the components of the external magnetic field and induced magnetic moment, respectively. The nuclear magnetic shielding isotropy σ is defined as [65]

$$\sigma = (\sigma_{xx} + \sigma_{yy} + \sigma_{zz})/3, \quad (12)$$

and the shielding anisotropy $\Delta\sigma$, an indication of the quality of the magnetic shielding tensor, is defined as [65]

$$\Delta\sigma = \sigma_3 - (\sigma_1 + \sigma_2)/2, \quad (13)$$

where $\sigma_1 < \sigma_2 < \sigma_3$ are the eigenvalues of the symmetrized shielding tensor. The nuclear magnetic shielding difference, or say, chemical shift δ , is reported in ppm (i.e., parts per million) and given by [65]

$$\delta = \left(\sigma^{(reference)} - \sigma^{(sample)} \right) \times 10^6, \quad (14)$$

where $\sigma^{(reference)}$ and $\sigma^{(sample)}$ denote the shielding isotropies σ for the reference and sample, respectively.

In both DFT and HF theory, the expression for the nuclear magnetic shielding tensor of nucleus X is given by [145]

$$\sigma_{ik} = \langle \Pi_{ik} O \rangle + \langle \theta_k \frac{\partial O}{\partial B_k} \rangle \quad (15)$$

with

$$\Pi_{ik} = \langle \Phi_\mu | \frac{\mathbf{r} \cdot (\mathbf{r} - \mathbf{R}_X) \delta_{ik} - r_i (\mathbf{r} - \mathbf{R}_X)_k}{2c^2 |\mathbf{r} - \mathbf{R}_X|^3} | \Phi_\nu \rangle; \quad (16)$$

$$\theta_k = \langle \Phi_\mu | -\frac{i[(\mathbf{r} - \mathbf{R}_X) \times \nabla]_k}{c |\mathbf{r} - \mathbf{R}_X|^3} | \Phi_\nu \rangle, \quad (17)$$

where c is the velocity of light, O is the density matrix, Φ_μ and Φ_ν are spin orbitals, \mathbf{R}_X is the position vector of nuclear X, and \mathbf{r} is the real space vector. In the above equation, $\partial O / \partial B_k$ is the derivative of the density matrix O with respect to the k th component of the magnetic field \mathbf{B} and is obtained via solution of the coupled-perturbed equations [145] for the appropriate perturbation. As gauge-invariance is achieved in different ways, the GIAO and CSGT methods differ at this point in the formation of the coupled-perturbed equations [145].

Table XIII: RHF and B3LYP calculations of the absolute isotropy (σ , in ppm) and anisotropy ($\Delta\sigma$, in ppm) of the carbon and nitrogen shielding tensors with a variety of Pople-style basis sets for $C_{48}N_{12}$ aza-fullerene, C_{60} and tetramethylsilane (TMS) by using the GIAO method. Numbers in the parenthesis for C_{60} are the relative errors of the calculated ^{13}C NMR shift δ to the NMR chemical shift $\delta^{exp.} = 142.7$ ppm measured by Taylor *et al.* [149].

Method	Molecule	Site Numbers $\{n_i\}$	Nuclei	STO-3G		3-21G		6-31G		6-31G*	
				σ	$\Delta\sigma$	σ	$\Delta\sigma$	σ	$\Delta\sigma$	σ	$\Delta\sigma$
RHF	$C_{48}N_{12}$	{1, 13, 16, 31, 38, 51}	^{13}C	91.5	155.5	65.9	155.6	44.0	173.0	48.5	168.3
		{2, 12, 29, 32, 37, 52}	^{13}C	109.8	156.7	89.8	149.2	67.9	169.2	67.7	168.2
		{3, 11, 28, 33, 36, 53}	^{13}C	116.8	132.2	99.2	123.5	76.6	141.2	88.5	126.9
		{4, 15, 27, 34, 40, 54}	^{13}C	103.5	141.9	75.8	139.0	57.9	154.9	46.9	156.7
		{5, 14, 30, 35, 39, 55}	^{15}N	193.7	134.8	142.7	143.8	114.4	171.5	140.7	128.5
		{6, 18, 24, 42, 48, 58}	^{13}C	120.2	104.8	101.6	89.8	78.2	110.5	89.6	82.5
		{7, 19, 23, 43, 47, 57}	^{13}C	106.2	135.9	80.6	131.0	59.4	152.2	54.2	148.7
		{8, 20, 22, 44, 46, 56}	^{13}C	111.5	140.9	94.6	126.1	70.7	150.8	82.9	131.1
		{9, 21, 26, 45, 50, 60}	^{15}N	182.7	151.6	132.6	167.7	95.3	202.6	121.7	170.4
		{10, 17, 25, 41, 49, 59}	^{13}C	104.9	125.2	80.0	117.0	59.5	133.5	55.1	126.9
	C_{60}	{1, 2, 3, 4, 5, 6, ..., 60}	^{13}C	101.8	156.6	74.0	162.7	54.1	180.1	54.7	178.8
	TMS	carbon site	^{13}C	238.5	5.6	208.3	16.9	200.8	21.4	195.1	17.5
	NH ₃	nitrogen site	^{15}N	306.9	9.2	271.1	17.5	264.4	18.2	260.8	17.4
C_{60}	Calculated ^{13}C NMR shift δ		136.7	(4.2%)	134.3	(5.9%)	146.7	(2.8%)	140.4	(1.6%)	
B3LYP	$C_{48}N_{12}$	{1, 13, 16, 31, 38, 51}	^{13}C	103.9	109.5	70.9	117.5	53.3	128.0	51.9	130.4
		{2, 12, 29, 32, 37, 52}	^{13}C	114.6	121.9	84.6	123.6	66.4	138.1	62.8	138.9
		{3, 11, 28, 33, 36, 53}	^{13}C	120.6	101.1	91.8	98.6	74.5	110.9	72.9	107.3
		{4, 15, 27, 34, 40, 54}	^{13}C	113.3	103.6	82.8	104.6	66.3	117.1	61.8	113.9
		{5, 14, 30, 35, 39, 55}	^{15}N	173.2	126.2	116.4	143.2	92.8	155.4	103.8	139.3
		{6, 18, 24, 42, 48, 58}	^{13}C	123.5	70.4	92.5	66.5	76.1	76.4	74.3	63.0
		{7, 19, 23, 43, 47, 57}	^{13}C	114.1	96.4	80.6	100.2	63.0	76.4	57.4	114.0
		{8, 20, 22, 44, 46, 56}	^{13}C	119.5	101.7	90.5	104.7	73.8	116.2	72.3	116.2
		{9, 21, 26, 45, 50, 60}	^{15}N	171.7	121.9	110.4	142.2	84.0	157.5	91.2	146.7
		{10, 17, 25, 41, 49, 59}	^{13}C	113.9	121.9	82.0	84.6	65.6	94.4	61.7	90.0
	C_{60}	{1, 2, 3, 4, 5, 6, ..., 60}	^{13}C	106.1	125.8	70.2	139.3	53.6	152.2	50.5	154.2
	TMS	carbon site	^{13}C	225.3	9.6	197.6	20.0	188.3	25.2	183.8	22.3
	NH ₃	nitrogen site	^{15}N	291.3	7.3	262.6	18.9	256.8	21.0	254.9	19.3
C_{60}	Calculated ^{13}C NMR shift δ		119.2	(16.5%)	127.4	(10.7%)	134.7	(5.6%)	133.3	(6.6%)	
Experiment	C_{60}	^{13}C NMR chemical shift δ from Taylor <i>et al.</i> [149]:									142.7
	TMS	absolute shielding isotropy σ for ^{13}C from Jameson <i>et al.</i> [148]:									188.1
	NH ₃	absolute shielding isotropy (σ) / anisotropy ($\Delta\sigma$) for ^{15}N from Ref. [150,151]:									264.5/20

The GIAO method uses the following explicit field-dependent basis functions for calculating the magnetic shielding tensor:

$$|\Phi_\mu(\mathbf{B})\rangle = e^{-i(\mathbf{B} \times \mathbf{r}_\mu) \cdot \mathbf{r} / (2c)} |\Phi_\mu(0)\rangle, \quad (18)$$

where \mathbf{r}_μ is the position vector of basis function Φ_μ and $\Phi_\mu(0)$ denotes the usual field-independent basis functions. In this method, three sets of the coupled-perturbed equations [145] are solved, one for each direction of the magnetic field.

In the CSGT method, the gauge-invariance is achieved from accurate calculations of the induced first-order electronic current density $\mathbf{J}^{(1)}(\mathbf{r})$ by performing a gauge transformation for each point in space. The nuclear magnetic shielding tensor is expressed in terms of $\mathbf{J}^{(1)}(\mathbf{r})$, i.e.,

$$\sigma_{ik} = -\frac{1}{Bc} \int \left[\frac{\mathbf{R}_X \times \mathbf{J}_k^{(1)}(\mathbf{r})}{R_X^3} \right]_i d\mathbf{R}_X, \quad (19)$$

Table XIV: RHF and B3LYP calculations of the absolute isotropy (σ , in ppm) and anisotropy ($\Delta\sigma$, in ippm) of the carbon and nitrogen shielding tensors with a variety of Pople-style basis sets for $C_{48}N_{12}$ aza-fullerene, C_{60} and tetramethylsilane (TMS) by using CSGT methods. Numbers in the parenthesis for C_{60} are the relative errors of the calculated ^{13}C NMR shift δ to the NMR chemical shift $\delta^{exp.} = 142.7$ ppm measured by Taylor *et al.* [149].

Method	Molecule	Site Numbers $\{n_i\}$	Nuclei	STO-3G		3-21G		6-31G		6-31G*	
				σ	$\Delta\sigma$	σ	$\Delta\sigma$	σ	$\Delta\sigma$	σ	$\Delta\sigma$
RHF	$C_{48}N_{12}$	{1, 13, 16, 31, 38, 51}	^{13}C	45.3	125.0	60.7	151.5	30.7	168.9	41.3	170.1
		{2, 12, 29, 32, 37, 52}	^{13}C	55.8	127.0	84.1	143.8	54.0	162.1	60.4	168.3
		{3, 11, 28, 33, 36, 53}	^{13}C	60.0	114.0	91.2	122.4	60.9	139.1	78.9	129.8
		{4, 15, 27, 34, 40, 54}	^{13}C	52.9	119.5	68.8	138.7	41.1	155.5	39.2	160.4
		{5, 14, 30, 35, 39, 55}	^{13}N	78.0	134.0	120.4	154.3	86.3	176.5	128.2	136.4
		{6, 18, 24, 42, 48, 58}	^{13}C	63.8	97.9	89.8	96.5	59.3	115.5	79.8	87.3
		{7, 19, 23, 43, 47, 57}	^{13}C	55.5	113.5	72.2	130.9	43.2	149.5	46.5	150.5
		{8, 20, 22, 44, 46, 56}	^{13}C	58.6	118.0	84.9	125.5	52.4	150.1	73.7	135.2
		{9, 21, 26, 45, 50, 60}	^{13}N	74.0	144.8	116.0	170.8	72.2	203.6	112.2	173.1
		{10, 17, 25, 41, 49, 59}	^{13}C	55.3	107.8	73.1	118.7	43.3	136.9	47.3	129.5
	C_{60}	{1, 2, 3, 4, 5, 6, ..., 60}	^{13}C	50.2	128.8	71.2	156.1	43.3	172.7	48.9	178.6
	TMS	carbon site	^{13}C	131.9	9.5	191.0	6.3	185.5	13.1	190.6	13.7
	NH ₃	nitrogen site	^{13}N	148.1	18.6	200.2	5.1	209.2	6.3	228.4	6.6
C_{60}	Calculated ^{13}C NMR shift δ		81.7 (42.7%)		119.8 (16.0%)		142.2 (0.4%)		141.7 (0.7%)		
B3LYP	$C_{48}N_{12}$	{1, 13, 16, 31, 38, 51}	^{13}C	58.6	86.4	66.0	114.1	39.1	126.6	45.7	131.8
		{2, 12, 29, 32, 37, 52}	^{13}C	66.1	94.8	81.7	119.3	53.9	133.5	57.2	139.6
		{3, 11, 28, 33, 36, 53}	^{13}C	69.3	83.5	87.2	99.0	60.3	111.1	66.3	109.4
		{4, 15, 27, 34, 40, 54}	^{13}C	64.6	84.8	75.8	104.0	49.1	118.5	54.7	117.6
		{5, 14, 30, 35, 39, 55}	^{13}N	78.5	116.6	104.9	142.0	74.6	152.7	96.8	142.4
		{6, 18, 24, 42, 48, 58}	^{13}C	71.9	63.6	84.1	72.0	58.7	81.9	66.9	66.5
		{7, 19, 23, 43, 47, 57}	^{13}C	66.5	77.7	73.8	99.7	47.5	112.2	51.0	115.3
		{8, 20, 22, 44, 46, 56}	^{13}C	70.4	81.9	83.5	101.7	56.7	115.8	65.7	118.7
		{9, 21, 26, 45, 50, 60}	^{13}N	81.6	112.8	103.4	140.2	69.3	156.6	86.0	148.5
		{10, 17, 25, 41, 49, 59}	^{13}C	66.9	71.6	76.1	88.1	49.5	100.1	54.8	93.8
	C_{60}	{1, 2, 3, 4, 5, 6, ..., 60}	^{13}C	58.2	100.3	69.2	134.7	43.1	148.4	45.9	149.2
	TMS	carbon site	^{13}C	124.9	10.0	181.7	9.0	175.0	16.5	181.6	18.0
	NH ₃	nitrogen site	^{13}N	137.7	27.1	190.0	9.6	200.4	6.0	221.5	6.5
C_{60}	Calculated ^{13}C NMR shift δ		66.7 (53.3%)		112.5 (21.2%)		131.9 (7.6%)		135.7 (4.9%)		

where B is the magnitude of magnetic field. Since the basis functions do not depend on the magnetic field, only six sets of the coupled-perturbed equations [145] are left and

solved (three for the components of the angular momentum perturbation using any single gauge origin, and three for the linear momentum perturbation resulting from any

single shift in gauge origin). Furthermore, the shielding tensors are obtained via Becke’s multi-center numerical integration scheme [147]

B. Results

The above mentioned GIAO and CSGT methods have been implemented into the Gaussian 98 program [73,72] and all calculations in this section are performed using this program.

Here we perform RHF and B3LYP hybrid DFT calculations of the nuclear magnetic shielding tensor of carbon and nitrogen atoms in $C_{48}N_{12}$, C_{60} , and tetramethylsilane (TMS [148]) by using GIAO and CSGT methods with STO-3G, 3-21G, 6-31G and 6-31G* basis sets. Calculation performed with a specific basis set and *ab initio* method use geometry optimized with the same basis set and *ab initio* method (see section II). Detailed results are summarized in Table XIII and XIV. Since no present functional includes a magnetic field dependence, the DFT methods do not provide systematically better shielding results than RHF [72]. Nevertheless, we also list the DFT results in Table XIII and XIV for comparison. The isotropic NMR chemical shifts δ relative to that of TMS are also shown in Table XIII and XIV. It is seen that the NMR shielding tensors for $C_{48}N_{12}$ are separated into eight groups for carbon atom and two groups for nitrogen atoms, i.e., eight ^{13}C and two ^{15}N NMR spectral signals are predicted. In contrast, C_{60} has only one ^{13}C NMR signal which is in agreement with experiment [149]. The experimental values of the absolute shielding constant σ for ^{15}N in NH_3 and ^{13}C in TMS, as shown in Table XIII and XIV, are 264.5 ppm [150,151] and 188.1 ppm [148], and our best calculated results for those reference materials are in good agreement with the experiments.

Table XIII and XIV also demonstrate the convergence of the GIAO and CSGT methods with respect to basis set for absolute shielding constants calculated with RHF and B3LYP hybrid DFT methods. For each first principles method, the shielding constants calculated with GIAO and CSGT methods are found to converge to almost the same values for the large basis set 6-31G*. NMR chemical shifts, as opposed to the absolute shielding constants σ , are measured with high accuracy in applications of NMR spectroscopy. On the other hand, calculated chemical shifts are in better agreement with experiment as relative differences are better represented [145]. Hence, given the absolute shielding constants for ^{13}C and ^{15}N in reference materials, i.e., TMS and NH_3 shown in Table XIII and XIV, we are able to calculate the chemical shifts δ and compare them with the experiments. For C_{60} , we find that the NMR chemical shifts δ calculated with the CSGT method at the RHF/6-31G and RHF/6-31G* levels are in agreement with experiment ($\delta^{exp} = 142.7$ ppm measured by Taylor *et al.* [149]). This suggests that CSGT method would predict NMR spec-

tral signals much better than GIAO. However, CSGT costs more CPU times than GIAO on the same machine, for example, about 5 hours more for RHF/6-31G* and 2 hours for B3LYP/6-31G* in the CSGT method.

To predict accurate NMR chemical shifts for large molecules, it is necessary to assess the accuracy of the available *ab initio* methods by employing lower levels of theory and by using basis sets as small as possible [145]. The results in Table XIII and XIV indicate that the RHF method yields better chemical shifts than the B3LYP hybrid DFT method, especially, for GIAO method and the minimum basis set STO-3G. As shown in Table XIII, the ^{13}C chemical shift in C_{60} differs from experiment by 23.5 ppm at the B3LYP level, while it differs by only 6 ppm at the RHF level of theory. Also it is noted that RHF makes positive and negative errors, while B3LYP makes only positive errors.

In addition, nuclear magnetic shielding anisotropies $\Delta\sigma$ are reported in Table XIII and XIV. Although these properties usually cannot be determined experimentally in the gas phase (except in cases where the high symmetry of the molecule together with the calculated diamagnetic contribution to the shielding tensor allows the determination of the anisotropy from the spin rotation [152]), these values are of interest. Anisotropies can be determined in solid state NMR experiments and calculations are often important for a correct assignment. From Table XIII and XIV, we find that the shielding anisotropies $\Delta\sigma$ for ^{15}N in NH_3 calculated with GIAO method with both *ab initio* theories are in good agreement with experiment, while those calculated with CSGT agree poorly with experiment.

VII. SUMMARY AND OUTLOOK

In summary, we have performed *ab initio* calculations of the structures, electronic properties, vibrational frequencies, IR intensities, NMR shielding tensors, linear polarizabilities, first- and second-order hyperpolarizabilities of the $C_{48}N_{12}$ aza-fullerene. Calculated results of $C_{48}N_{12}$ are compared with those of C_{60} at the same level of theory. It is found that this aza-fullerene has some remarkable features, which are different from and can compete with C_{60} . The detailed studies of C_{60} show the importance of electron correlations and the choice of basis sets in the *ab initio* calculations. Our best results for C_{60} obtained with the B3LYP hybrid DFT method are in excellent agreement with experiment and demonstrate the needed efficiency and accuracy of this method for obtaining quantitative information on the structural, electronic and vibrational properties of these materials.

Laser sources are widely used in the laboratory and industry. However, they are a potential hazard for eyes, thermal cameras and other optical sensors [10,11,153]. Development of optical limiters which can suppress undesired radiation and effectively decrease transmittance

at high intensity or fluence is necessary. An ideal optical limiter [10,153] should have reasonable linear transmittance at low input fluence (at least of 70%), protecting optical sensors or eyes against laser pulses of any wavelength and pulse duration, and its output energy must remain below the optical damage threshold of sensors or eyes at high fluences. C_{60} and fullerene derivatives are good candidates for optical limiting applications [10,154,155]. In this paper, we found that the average second-order hyperpolarizability of $C_{48}N_{12}$ is about 55% larger than that of C_{60} . Hence, it is expected that $C_{48}N_{12}$ is also a good candidate for optical limiting applications.

Non-linear optical (NLO) materials have vast technological applications in telecommunications, optical data storage and optical information processing. The search for materials with such properties is the subject of intense research [9,10,156]. Organic molecules, which have high NLO response, could be designed by linking appropriate electron-donor and acceptor groups with a spacer made of one or several units of conjugated molecules such as a polyene or an aromatic chain [156]. Based on such donor-acceptor model, we can link donor $C_{48}N_{12}$ and acceptor C_{60} with a polyene or an aromatic chain and design one kind of organic molecules. In such organic molecules, charge would migrate from $C_{48}N_{12}$ to C_{60} upon electronic excitation, giving rise to a large dipole moment along the direction connecting the donor/acceptor pair. Thus, large NLO response is expected in these donor/acceptor-based molecules.

Carbon nanotubes are promising materials for building electronic devices, in particular, field effect transistors (FETs) [11,157]. However, single-walled carbon nanotube (SWNT) FETs built from as-grown tubes are unipolar p -type, i.e., there is no electron current flow even at large positive gate biases. This behavior suggests the presence of a Schottky barrier at the metal-nanotube contact. Obviously, the capability to produce n -type transistors is important technologically, as it allows the fabrication of nanotube-based complementary logic devices and circuits [158,159]. Very recently, Bockrath *et al.* [160] have reported a controlled chemical doping of individual semiconducting SWNT ropes by reversibly intercalating and deintercalating potassium. Potassium doping could change the carriers in the ropes from holes to electrons [160]. Their experiments open the way toward other experiments that require controlled doping such as making nanoscale p - n junctions. As shown in this paper, $C_{48}N_{12}$ is a good electron donor. We found that incorporating $C_{48}N_{12}$ into a (10,10) semiconducting SWNT [7] would result in $-0.26 e$ charge [90] on the nanotube forming a n -type SWNT-based transistor.

To obtain molecular rectification, the LUMO of the acceptor should lie at or slightly above the Fermi level of the electrode and above the HOMO of the donor [161]. Hence it is important to search for desired donor/acceptor pairs which satisfy those conditions. The acceptor/donor pair, $C_{48}B_{12}/C_{48}N_{12}$, actually is demonstrated to be an ideal candidate for molecular electronics [90]. For example,

we have shown that a rectifier formed by $C_{48}B_{12}/C_{48}N_{12}$ pair shows a perfect rectification behavior [90].

As shown before, $C_{48}B_{12}$ and $C_{48}N_{12}$ fcc solids are semiconducting materials. Because both $C_{48}B_{12}$ and $C_{48}N_{12}$ molecules have opposite electronic polarizations, it is possible to use them to build semiconducting materials with opposite electronic polarizations.

Therefore, $C_{48}N_{12}$ could have potential applications as semiconductor components, nonlinear optical materials, and possible building materials for molecular electronics and photonic devices. Efficiently synthesizing $C_{48}N_{12}$ would be of great experimental interest within reach of today's technology.

ACKNOWLEDGEMENTS

We thank Dr. Denis A. Lehané and Dr. Hartmut Schmider for their technical help. One of us (R. H. X.) thanks the HPCVL (High Performance Computing Virtual Laboratory) at Queen's University for the use of its parallel supercomputing facilities. L.J. gratefully acknowledges the Danish Research Training Council for financial support. J.Z. acknowledges support from the University Research Council of University of North Carolina at Chapel Hill. VHS gratefully acknowledges support from the Natural Science and Engineering Research Council of Canada(NSERC).

-
- [1] G. Benedek, P. Milani, and V. G. Ralchenko (eds.), *Nanostructured Carbon for Advanced Applications* (Kluwer, Dordrecht, 2001).
 - [2] A. A. Lucas, F. Moreau, and Ph. Lambin, *Rev. Mod. Phys.* **74**, 1 (2002).
 - [3] H. W. Kroto, J. R. Heath, S. C. O'Brien, R. F. Curl, and R. E. Smalley, *Nature* (London) **318**, 162 (1985).
 - [4] R. F. Curl and R. E. Smalley, *Sci. Am.* **264**, 54 (1991).
 - [5] W. Krätschmer, L. D. Lamb, K. Fostiropoulos, and D. R. Huffman, *Nature* (London) **347**, 354 (1990).
 - [6] D. R. Huffman, *Phys. Today* **44**, 22 (1991).
 - [7] M. S. Dresselhaus, G. Dresselhaus, and P. C. Eklund, *Science of Fullerenes and Carbon Nanotubes* (Academic Press, New York, 1996).
 - [8] W. Andreoni (ed.), *The Physics of Fullerene-Based and Fullerene-Related Materials* (Kluwer, New York, 2000)
 - [9] R. H. Xie, "Nonlinear Optical Properties of Fullerenes and Carbon Nanotubes", in: *Handbook of Advanced Electronic and Photonic Materials and Devices, Vol. 9: Nonlinear Optical Materials*, H. S. Nalwa (Ed.) (Academic Press, New York, 2000), pp.267-307.
 - [10] R.H. Xie, Q. Rao, and L. Jensen, "Nonlinear Optics of Fullerenes and Carbon Nanotubes", in: *Encyclopedia of Nanoscience and Nanotechnology*, H.S. Nalwa (Ed.) (American Scientific Publisher, California, 2003).

- [11] R.H. Xie, J. Zhao, and Q. Rao, "Doped Carbon Nanotubes", in: *Encyclopedia of Nanoscience and Nanotechnology*, H.S. Nalwa (Ed.) (American Scientific Publisher, California, 2003).
- [12] E. Osawa (ed.), *Perspectives of Fullerene Nanotechnology* (Kluwer, New York, 2002).
- [13] K. Holczer, O. Klein, S. M. Huang, R. B. Kaner, K. J. Fu, R. L. Whetten, and F. Diederich, *Science* **252**, 1154 (1991).
- [14] D. T. On, L. Jiang, K. Kitazawa, A. Fujishima, and K. Hashimoto, *J. Phys. Chem. B* **103**, 3511 (1999).
- [15] T. Guo, C. M. Jin, and R. E. Smalley, *J. Phys. Chem.* **95**, 4948 (1991).
- [16] J. C. Hummelen, B. Knight, J. Pavlovich, R. González, and F. Wudl, *Science* **269**, 1554 (1995).
- [17] W. Andreoni, A. Curioni, K. Holczer, K. Prassides, M. Keshavarz-K, J.C. Hummelen, and F. Wudl, *J. Am. Chem. Soc.* **118**, 11335 (1996).
- [18] L. Hultman, S. Stafström, Z. Czigány, J. Neidhardt, N. Hellgren, I. F. Brunell, K. Suenaga, and C. Coolix, *Phys. Rev. Lett.* **87**, 225503 (2001).
- [19] S. Stafström, L. Hultman, and N. Hellgren, *Chem. Phys. Lett.* **340**, 227 (2001).
- [20] R.H. Xie, G.W. Bryant, and V.H. Smith, Jr., *Chem. Phys. Lett.* **368**, 486 (2002).
- [21] J. Cioslowski, *Electronic Structure Calculations on Fullerenes and Their Derivatives* (Oxford University Press, New York, 1995).
- [22] G. E. Scuseria, *Science* **271**, 942 (1996).
- [23] D. B. Cook, *Handbook of Computational Quantum Chemistry* (Oxford University Press, New York, 1998).
- [24] P. R. Taylor, E. Bylaska, J. H. Weare, and R. Kawai, *Chem. Phys. Lett.* **235**, 558 (1995).
- [25] R. L. Disch and J. M. Schulmann, *Chem. Phys. Lett.* **125**, 465 (1986).
- [26] H. P. Lüthi and J. Almlöf, *Chem. Phys. Lett.* **135**, 357 (1987).
- [27] G. Scuseria, *Chem. Phys. Lett.* **176**, 423 (1991).
- [28] M. Häser, J. Almlöf, and G. E. Scuseria, *Chem. Phys. Lett.* **181**, 497 (1991).
- [29] N. Kurita, K. Kobayashi, H. Kumahara, and K. Tago, *Phys. Rev. B* **48**, 4850 (1993).
- [30] J. Hrusák and H. Schwarz, *Chem. Phys. Lett.* **205**, 187 (1993).
- [31] D. Bakowies, M. Bühl, and W. Thiel, *Chem. Phys. Lett.* **247**, 491 (1995).
- [32] J. Cioslowski, N. Rao, and D. Moncrieff, *J. Am. Chem. Soc.* **124**, 8485 (2002).
- [33] P. Hohenberg and W. Kohn, *Phys. Rev.* **136**, B864 (1964).
- [34] W. Kohn and L. J. Sham, *Phys. Rev.* **140**, A1133 (1965).
- [35] G. E. Scuseria, *Chem. Phys. Lett.* **243**, 193 (1995).
- [36] R. W. Boyd, *Nonlinear Optics* (Academic Press, New York, 1992).
- [37] M. Bianchetti, P. F. Buonsante, F. Ginelli, H. E. Roman, R. A. Broglia, and F. Alasia, *Phys. Reports* **357**, 459 (2002).
- [38] L. A. Woodward, *Introduction to the Theory of Molecular Vibrations and Vibrational Spectroscopy* (Oxford University Press, London, 1972).
- [39] N. B. Colthup, L. H. Daly, and S. E. Wiberley, *Introduction to Infrared and Raman Spectroscopy* (3rd Ed.) (Academic Press, New York, 1990).
- [40] W. Krätschmer, K. Fostiropoulos, and D. R. Huffman, *Chem. Phys. Lett.* **170**, 167 (1990).
- [41] D. S. Bethune, G. Meijer, W. C. Tang, H. J. Rosen, W. G. Golden, H. Seki, C. A. Brown, and M. S. de Vries, *Chem. Phys. Lett.* **179**, 181 (1991).
- [42] K. A. Wang, A. M. Rao, P. C. Eklund, M. S. Dresselhaus, and G. Dresselhaus, *Phys. Rev. B* **48**, 11375 (1993).
- [43] M. C. Martin, X. Du, J. Kwon, and L. Mihaly, *Phys. Rev. B* **50**, 173 (1994).
- [44] K. A. Wang, Y. Wang, P. Zhou, J. M. Holden, S. L. Ren, G. T. Hager, H. F. Ni, P. C. Eklund, G. Dresselhaus, and M. S. Dresselhaus, *Phys. Rev. B* **45**, R1955 (1992).
- [45] K. Lynch, C. Tanke, F. Menzel, W. Brockner, P. Scharff and E. Stumpp, *J. Phys. Chem.* **99**, 7985 (1995).
- [46] P. Zhou, K. A. Wang, Y. Wang, P. C. Eklund M. S. Dresselhaus, G. Dresselhaus, and R. A. Jishi, *Phys. Rev. B* **46**, 2595 (1992).
- [47] Z. H. Dong, P. Zhou, J. M. Holden, P. C. Eklund, M. S. Dresselhaus, and G. Dresselhaus, *Phys. Rev. B* **48**, R2862 (1993).
- [48] S. Guha, J. Menéndez, J. B. Page, G. B. Adams, G. S. Spencer, J. P. Lehman, P. Giannozzi, and S. Baroni, *Phys. Rev. Lett.* **72**, 3359 (1994).
- [49] P. J. Horowski, M. L. W. Thewalt, and T. R. Anthony, *Phys. Rev. Lett.* **74**, 194 (1995).
- [50] P. Giannozzi and W. Andreoni, *Phys. Rev. Lett.* **76**, 4915 (1996).
- [51] K. Pokhodnia, J. Demsar, A. Omerzu, D. Mihailovic, and H. Kuzmany, *Phys. Rev. B* **55**, 3757 (1997).
- [52] A. M. Rao, P. C. Eklund, J-L. Hodeau, L. Marques, and M. Nunez-Regueiro, *Phys. Rev. B* **55**, 4766 (1997).
- [53] M. F. Limonov, Yu. E. Kitaev, A. V. Chugreev, V. P. Smirnov, Yu. S. Grushko, S. G. Kolesnik, and S. N. Kolesnik, *Phys. Rev. B* **57**, 7586 (1998).
- [54] X. H. Chen, T. Takenobu, T. Muro, H. Fudo, and Y. Iwasa, *Phys. Rev. B* **60**, 12462 (1999).
- [55] V. A. Davydov, L. S. Kashevarova, A. V. Rakhmanina, V. M. Senyavin, R. Céolin, H. Szwarc, H. Allouchi, and V. Agafonov, *Phys. Rev. B* **61**, 11936 (2000).
- [56] I. D. Hands, J. L. Dunn, and C. A. Bates, *Phys. Rev. B* **63**, 245414 (2001).
- [57] A. V. Talyzin, L. S. Dubrovinsky, T. Le Bihan, and U. Jansson, *Phys. Rev. B* **65**, 245413 (2002).
- [58] A. M. Rao, P. C. Eklund, S. Bandow, A. Thess, and R. E. Smalley, *Nature (London)* **388**, 257 (1997).
- [59] A. M. Rao, E. Richter, S. Bandow, B. Chase, P. C. Eklund, K. A. Williams, S. Fang, K. R. Subbaswamy, M. Menon, A. Thess, R. E. Smalley, G. Dresselhaus, and M. S. Dresselhaus, *Science* **275**, 187 (1997).
- [60] N. Bendiab, E. Anglaret, J. L. Bantignies, A. Zahab, J. L. Sauvajol, P. Petit, C. Mathis, and S. Lefrant, *Phys. Rev. B* **64**, 245424 (2001).
- [61] U. D. Venkateswaran, E. A. Brandsen, M. E. Katakowski, A. Harutyunyan, G. Chen, A. L. Loper,

- and P. C. Eklund, Phys. Rev. B **65**, 054102 (2002).
- [62] W. Zhou, S. Xie, L. Sun, D. Tang, Y. Li, Z. Liu, L. Ci, Z. Zou, G. Wang, P. Tan, X. Dong, B. Xu, and B. Zhao, Appl. Phys. Lett. **80**, 2553 (2002).
- [63] M. E. Itkis, S. Niyogi, M. E. Meng, M. A. Hamon, H. Hu, and R. C. Haddon, Nano Lett. **2**, 155 (2002).
- [64] K. A. Williams, B. K. Pradhan, P. C. Eklund, M. K. Kostov, and M. W. Cole, Phys. Rev. Lett. **88**, 165502 (2002).
- [65] I. Ando and G. A. Webb, *Theory of NMR Parameters* (Academic Press, New York, 1983).
- [66] R. J. Abraham, J. Fisher and P. Loftus, *Introduction to NMR Spectroscopy* (Chichester, New York, 1988).
- [67] B. D. N. Rao and M. D. Kemple, *NMR as a Structural Tool for Macromolecules: Current Status and Future Directions* (Plenum Press, New York, 1996).
- [68] N. S. Ramsey, Phys. Rev. **78**, 699 (1950).
- [69] N. S. Ramsey, Phys. Rev. **91**, 303 (1953).
- [70] F. London, J. Phys. Radium (Paris) **8**, 397 (1937).
- [71] T. A. Keith and R. F. W. Bader, Chem. Phys. Lett. **210**, 223 (1993).
- [72] Gaussian 98, Revision A.9, M. J. Frisch, G. W. Trucks, H. B. Schlegel, G. E. Scuseria, M. A. Robb, J. R. Cheeseman, V. G. Zakrzewski, J. A. Montgomery, Jr., R. E. Stratmann, J. C. Burant, S. Dapprich, J. M. Millam, A. D. Daniels, K. N. Kudin, M. C. Strain, O. Farkas, J. Tomasi, V. Barone, M. Cossi, R. Cammi, B. Mennucci, C. Pomelli, C. Adamo, S. Clifford, J. Ochterski, G. A. Petersson, P. Y. Ayala, Q. Cui, K. Morokuma, D. K. Malick, A. D. Rabuck, K. Raghavachari, J. B. Foresman, J. Cioslowski, J. V. Ortiz, A. G. Baboul, B. B. Stefanov, G. Liu, A. Liashenko, P. Piskorz, I. Komaromi, R. Gomperts, R. L. Martin, D. J. Fox, T. Keith, M. A. Al-Laham, C. Y. Peng, A. Nanayakkara, M. Challacombe, P. M. W. Gill, B. Johnson, W. Chen, M. W. Wong, J. L. Andres, C. Gonzalez, M. Head-Gordon, E. S. Replogle, and J. A. Pople, Gaussian, Inc., Pittsburgh PA, 1998.
- [73] Use of this software does not constitute an endorsement or certification by NIST.
- [74] J. C. Slater, Phys. Rev. **36**, 57 (1930).
- [75] W. J. Hehre, R. F. Stewart, and J. A. Pople, J. Chem. Phys. **51**, 2657 (1969).
- [76] J. S. Binkley and J. A. Pople, J. Am. Chem. Soc. **102**, 939 (1980).
- [77] W. J. Hehre, R. Ditchfield, and J. A. Pople, J. Chem. Phys. **56**, 2257 (1972).
- [78] R. Krishnan, J. S. Binkley, R. Seeger, and J. A. Pople, J. Chem. Phys. **72**, 650 (1980).
- [79] M. J. Frisch, J. A. Pople, and J. S. Binkley, J. Chem. Phys. **80**, 3265 (1984).
- [80] A. D. Becke, J. Chem. Phys. **98**, 5648 (1993).
- [81] J. C. Slater, Phys. Rev. **81**, 385 (1951).
- [82] A. D. Becke, Phys. Rev. A **38**, 3098 (1988).
- [83] S. H. Vosko, L. Wilk, and M. Nusair, Can. J. Phys. **58**, 1200 (1980).
- [84] C. Lee, W. Yang, and R. G. Parr, Phys. Rev. B **37**, 785 (1988).
- [85] J. P. Perdew and Y. Wang, Phys. Rev. B **45**, 13244 (1992).
- [86] H. B. Bürgi, E. Blanc, D. Schwarzenbach, S. Liu, Y. Lu, M. M. Kappes, and J. A. Ibers, Angew. Chem. Int. Ed. Engl. **41**, 640 (1992).
- [87] K. P. Bohnen, R. Heid, K. M. Ho, and C. T. Chan, Phys. Rev. B **51**, 5805 (1995).
- [88] Q. M. Zhang, J. Y. Yi, and J. Bernholc, Phys. Rev. Lett. **66**, 2633 (1991).
- [89] A. Szabo and N. S. Ostlund, *Modern Quantum Chemistry* (Macmillan, New York, 1982).
- [90] R.H. Xie, G.W. Bryant, J. Zhao, V.H. Smith, Jr., A. Di Carlo, and A. Pecchia, unpublished.
- [91] W. I. F. David, R. M. Ibberson, J. C. Matthewman, K. Prassides, T. J. S. Dennis, J. P. Hare, H. W. Kroto, R. Taylor, and D. R. M. Walton, Nature (London) **353**, 147 (1991).
- [92] C. S. Yannoni, P. P. Bernier, D. S. Bethune, G. Maijer, and J. R. Salem, J. Am. Chem. Soc. **113**, 3190 (1991).
- [93] R. D. Johnson, G. Meijer, and D. S. Bethune, J. Am. Chem. Soc. **112**, 8983 (1990).
- [94] K. Hedberg, L. Hedberg, D. S. Bethune, C. A. Brown, H. C. Dorn, R. D. Johnson, and M. de Vries, Science **254**, 410 (1991).
- [95] R. C. Haddon, L. E. Brus, and K. Raghavachari, Chem. Phys. Lett. **125**, 459 (1986).
- [96] F. Negri, G. Orlandi, and F. Zerbetto, Chem. Phys. Lett. **144**, 31 (1988).
- [97] R. E. Stanton and M. D. Newton, J. Phys. Chem. **92**, 2141 (1988).
- [98] M. Kállay, K. Németh, and P. R. Surján, J. Phys. Chem. **102**, 1261 (1998).
- [99] X. Q. Wang, C. Z. Wang, and K. M. Ho, Phys. Rev. B **48**, 1884 (1993).
- [100] D. A. Dixon, B. E. Chase, G. Fitzgerald, and N. Matsuzawa, J. Phys. Chem. **99**, 4486 (1995).
- [101] T. Hara, J. Onoe, and K. Takeuchi, Phys. Rev. B **63**, 115412 (2001).
- [102] G. Onida, W. Andreoni, J. Kohanoff, and M. Parrinello, Chem. Phys. Lett. **219**, 1 (1994).
- [103] I. V. Hertel, H. Steger, J. DeVries, B. Weisser, C. Menzel, B. Kamke, and W. Kamke, Phys. Rev. Lett. **68**, 784 (1992).
- [104] R. K. Yoo, B. Ruscic, and J. Berkowitz, J. Chem. Phys. **96**, 911 (1992).
- [105] J. DeVries, H. Steger, B. Kamke, C. Menzel, B. Weisser, W. Kamke, and I. V. Hertel, Chem. Phys. Lett. **188**, 159 (1992).
- [106] H. Steger, J. Holzapfel, A. Hielscher, W. Kamke, and I. V. Hertel, Chem. Phys. Lett. **234**, 455 (1995).
- [107] C. Brink, L. H. Andersen, P. Hvelplund, D. Mathur, and J. D. Voldstad, Chem. Phys. Lett. **233**, 52 (1995).
- [108] X.B. Wang, C.F. Ding, and L.S. Wang, J. Chem. Phys. **110**, 8217 (1999).
- [109] R. W. Lof, M. A. van Veenendaal, B. Koopmans, H. T. Jonkman, and G. A. Sawatzky, Phys. Rev. Lett. **68**, 3924 (1992).
- [110] CASTEP, distributed by Accelrys Inc., is a DFT package based on plane-wave pseudopotential technique: M.C.Payne *et al.*, Rev. Mod. Phys. **64**, 1045 (1992).
- [111] R.M. Fleming, A.P. Ramirez, M.J. Rosseinsky, D.W. Murphy, R.C. Haddon, S.M. Zahurak, and A.V.

- Makhija, *Nature (London)*, **352**, 787 (1991).
- [112] R. Schwedhelm, L. Kipp, A. Dallmeyer, and M. Skibowski, *Phys. Rev. B* **58**, 13176 (1998).
- [113] ADF 2002.01., *Theoretical Chemistry Vrije Universiteit, Amsterdam* (2002).
- [114] G. te Velde, F. M. Bickelhaupt, E. J. Baerends, C. Fonseca Guerra, S. J. A. van Gisbergen, J. G. Snijders, and T. Ziegler. *J. Comp. Chem.*, **22**, 931 (2001).
- [115] G. D. Zeiss, W. R. Scott, N. Suzuki, and D. P. Chong, *Mol. Phys.* **37**, 1543 (1979).
- [116] L. Jensen, P. Th. van Duijnen, J. G. Snijders, and D. P. Chong, *Chem. Phys. Lett.* **359**, 524 (2002).
- [117] P. W. Fowler, P. Lazeretti, and R. Zanasi, *Chem. Phys. Lett.* **165**, 79 (1990).
- [118] D. J. Tozer and N. C. Handy, *J. Chem. Phys.* **109**, 10180 (1998).
- [119] M. R. Pederson and A. A. Quong, *Phys. Rev. B* **46**, 13584 (1992).
- [120] S. J. A. van Gisbergen, J. G. Snijders, and E. J. Baerends, *Phys. Rev. Lett.* **78**, 3097 (1997).
- [121] J.-I. Iwata, K. Yabana, and G. F. Bertsch, *J. Chem. Phys.* **115**, 8773 (2001).
- [122] C. Kittel, *Introduction to Solid State Physics* (Wiley, New York, 1976).
- [123] A. F. Hebard, R. C. Haddon, R. M. Fleming, and A. R. Korton, *Appl. Phys. Lett.* **59**, 2109 (1991).
- [124] P. Eklund, *Bull. Am. Phys. Soc.* **37**, 191 (1992).
- [125] A. A. Quong and M. R. Pederson, *Phys. Rev. B* **46**, 12906 (1992).
- [126] R. Antoine, Ph. Dugourd, D. Rayane, E. Benichou, M. Broyer, F. Chandezon, and C. Guet, *J. Chem. Phys.* **110**, 9771 (1999).
- [127] A. Ballard, K. Bonin, and J. Louderback, *J. Chem. Phys.* **113**, 5732 (2000).
- [128] S. J. A. van Gisbergen, J. G. Snijders, and E. J. Baerends, *J. Chem. Phys.* **109**, 10644 (1998).
- [129] S. J. A. van Gisbergen, J. G. Snijders, and E. J. Baerends, *J. Chem. Phys.* **109**, 10657 (1998).
- [130] S. J. A. van Gisbergen, J. G. Snijders, and E. J. Baerends, *Comput. Phys. Commun.* **118**, 119 (1999).
- [131] D. Jonsson, P. Norman, K. Ruud, H. Ågren, and T. Helgaker, *J. Chem. Phys.* **109**, 572 (1998).
- [132] E. B. Wilson, J. C. Decius, and P. C. Cross, *Molecular Vibrations* (McGraw-Hill, New York, 1955).
- [133] M. Cardona, in: *Light Scattering in Solids II*, Topics in Applied Physics, Vol.50 (Springer, Berlin, 1982).
- [134] G. Dresselhaus, M. S. Dresselhaus, and P. C. Eklund, *Phys. Rev. B* **45**, 6923 (1992).
- [135] A. Warshel and M. Karplus, *J. Am. Chem. Soc.* **94**, 5612 (1974).
- [136] Z. C. Wu, D. A. Jelski, and T. F. George, *Chem. Phys. Lett.* **137**, 291 (1987).
- [137] S. J. Cyvin, E. Brendsdal, B. N. Cyvin, and J. Brunvoll, *Chem. Phys. Lett.* **143**, 377 (1988).
- [138] D. E. Weeks and W. G. Harter, *J. Chem. Phys.* **90**, 4744 (1989).
- [139] R. A. Jishi, R. M. Mirie, and M. S. Dresselhaus, *Phys. Rev. B* **45**, 13685 (1992).
- [140] J. Onoe and K. Takeuchi, *Phys. Rev. B* **54**, 6167 (1996).
- [141] C.H. Choi, M. Kertesz, and L. Mihaly, *J. Phys. Chem. A* **104**, 102 (2000).
- [142] P. Pulay, G. Fogarasi, G. Pongor, J.E. Boggs, and A. Vargha, *J. Am. Chem. Soc.* **105**, 7037 (1983).
- [143] J. Gauss, *J. Chem. Phys.* **99**, 3629 (1993).
- [144] R. Ditchfield, *Mol. Phys.* **27**, 789 (1974).
- [145] J. R. Cheeseman, M. J. Frisch, G. W. Trucks, and T. A. Keith, *J. Chem. Phys.* **104**, 5497 (1996).
- [146] K. Wolinski, J. F. Hilton, and P. Pulay, *J. Am. Chem. Soc.* **112**, 8251 (1990).
- [147] A. D. Becke, *J. Chem. Phys.* **88**, 2547 (1988).
- [148] A. K. Jameson and C. J. Jameson, *Chem. Phys. Lett.* **134**, 461 (1987).
- [149] R. Taylor, J. P. Hare, A. K. Abdul-Sada, and H. W. Kroto, *J. Chem. Soc., Chem. Commun.*, 1423 (1990).
- [150] S. G. Kukolich, *J. Am. Chem. Soc.* **97**, 5704 (1975).
- [151] C. J. Jameson, A. K. Jameson, D. Oppusungu, S. Wille, and P. M. Burrell, *J. Chem. Phys.* **74**, 81 (1981).
- [152] J. Gauss and J. F. Stanton, *J. Chem. Phys.* **103**, 3561 (1995).
- [153] L. Vivien, P. Lancon, D. Riehl, F. Hache, and E. Anglaret, *Carbon* **40**, 1789 (2002).
- [154] L.W. Tutt and A. Kost, *Nature (London)* **356**, 225 (1991).
- [155] C. Liu, G. Zhao, Q. Gong, K. Tang, X. Jin, P. Cui, and L. Li, *Opt. Commun.* **184**, 309 (2000).
- [156] A.G.H. Barbosa and M.A.C. Nascimento, *Chem. Phys. Lett.* **343**, 15 (2001), and references therein.
- [157] R. Martel, T. Schmidt, H.R. Shea, T. Hertel, and Ph. Avouris, *Appl. Phys. Lett.* **73**, 2447 (1998).
- [158] V. Derycke, R. Martel, J. Appenzeller, and Ph. Avouris, *Nano Lett.* **1**, 453 (2001).
- [159] X. Liu, C. Lee, C. Zhou, and J. Han, *Appl. Phys. Lett.* **79**, 3329 (2001).
- [160] M. Bockrath, J. Hone, A. Zettl, P.L. McEuen, A.G. Rinzler, and R.E. Smalley, *Phys. Rev. B* **61**, 10606 (2000).
- [161] C. Joachim, J. K. Gimzewski, and A. Aviram, *Nature (London)* **408**, 541 (2000).